

1  
2  
3  
4  
5  
6  
7  
8  
9  
10  
11

# Coupled Feedbacks on the Northern Hemisphere Midlatitude Jet Response to 4xCO<sub>2</sub>: Changes in Stratospheric Ozone and the Atlantic Meridional Overturning Circulation

Clara Orbe<sup>1,2</sup>, David Rind<sup>1</sup>, Darryn Waugh<sup>3</sup>, Jeffrey Jonas<sup>1,4</sup>, Xiyue Zhang<sup>3</sup>,  
Gabriel Chiodo<sup>5</sup>, Larissa Nazarenko<sup>1,4</sup>, Gavin Schmidt<sup>1</sup>

<sup>1</sup>NASA Goddard Institute for Space Studies, New York, NY

<sup>2</sup>Department of Applied Physics and Applied Mathematics, Columbia University, New York, NY

<sup>3</sup>Department of Earth and Planetary Sciences, Johns Hopkins University, Baltimore, MD

<sup>4</sup>Center for Climate Systems Research, Earth Institute, Columbia University, New York, NY

<sup>5</sup>Institute for Atmospheric and Climate Science, ETH Zurich, Switzerland

12  
13  
14  
15  
16  
17  
18  
19  
20  
21  
22

## Key Points:

- The NH midlatitude jet response to 4xCO<sub>2</sub> is modulated by feedbacks from both changes in stratospheric ozone and a weakening of the Atlantic Meridional Overturning Circulation (AMOC).
- These feedbacks are coupled together as changes in stratospheric ozone drive an equatorward shift of the jet over the North Atlantic, which reduces heat fluxes into the ocean and North Atlantic Deep Water formation, resulting in a stronger decline of the AMOC under 4xCO<sub>2</sub> forcing.
- Changes in stratospheric ozone affect the NH jet on a “fast” (5-20 year) timescale, during which the jet shifts equatorward. By comparison, a weakening of the AMOC drives a poleward shift in the NH midlatitude jet on “long” (100-150 year) timescales.

---

Corresponding author: Clara Orbe, [clara.orbe@nasa.gov](mailto:clara.orbe@nasa.gov)

23 **Abstract**

24 Ozone, and its response to anthropogenic forcings, provide an important pathway  
 25 for the coupling between atmospheric composition and climate. This applies to strato-  
 26 spheric ozone as well as ozone in the troposphere; in addition to stratospheric ozone’s  
 27 radiative impacts, recent studies have shown that changes in the ozone layer due to  $4xCO_2$   
 28 have a considerable impact on the Northern Hemisphere (NH) tropospheric circulation,  
 29 inducing an equatorward shift of the North Atlantic jet during boreal winter. Here we  
 30 show that this equatorward jet shift induces a more rapid weakening of the Atlantic Merid-  
 31 ional Overturning Circulation (AMOC), resulting in a poleward shift of the jet on longer  
 32 timescales. As such, coupled feedbacks from both stratospheric ozone and the AMOC  
 33 result in a two-timescale response of the NH midlatitude jet to abrupt  $4xCO_2$  forcing:  
 34 a “fast” response (5-20 years) during which the North Atlantic jet shifts equatorward  
 35 and a “long” response ( $\sim 100$ -150 years) during which the jet shifts poleward. The lat-  
 36 ter is driven by a weakening of the AMOC that develops in response to weaker surface  
 37 zonal winds, that result in reduced heat fluxes out of the subpolar gyre, reducing North  
 38 Atlantic Deep Water formation. Our results suggest that stratospheric ozone changes  
 39 in the tropical lower stratosphere can have a surprisingly powerful effect on the AMOC,  
 40 independent of other aspects of climate change.

41 **Plain Language Summary**42 **1 Introduction**

43 There is large uncertainty in the atmospheric circulation response to increasing green-  
 44 house gases (e.g., Shepherd (2014)). Although models generally predict a poleward shift  
 45 of the westerly jet, the magnitude of this shift is highly uncertain (e.g., Vallis et al. (2015);  
 46 Grise and Polvani (2014)) as are its underlying drivers (T. A. Shaw (2019)). This is es-  
 47 pecially true in the Northern Hemisphere (NH), where there are opposing thermodynamic  
 48 influences, i.e. opposite meridional temperature gradient responses at the surface ver-  
 49 sus the upper troposphere (T. Shaw et al. (2016)). Thus, while enhanced warming in the  
 50 lower polar troposphere relative to the lower tropical troposphere (i.e., Arctic amplifi-  
 51 cation) contributes to reduced meridional temperature gradients, increases in upper tro-  
 52 pospheric tropical warming contribute to enhanced temperature gradients aloft (Butler  
 53 et al. (2010); Yuval and Kaspi (2020)) and it is not clear how these competing processes  
 54 affect the zonal mean jet.

55 Many processes have been shown to influence the response of meridional temper-  
 56 ature gradients to increased  $CO_2$ , including polar amplification (see Smith et al. (2019)  
 57 and references therein) and cloud feedbacks (e.g., Ceppi and Hartmann (2015); Voigt and  
 58 Shaw (2015)). By comparison, composition feedbacks associated with the ozone response  
 59 to  $CO_2$  have been less well examined although stratospheric ozone changes have been  
 60 identified as an important pathway coupling composition to climate (Isaksen et al. (2009)).  
 61 In particular, the stratospheric ozone response to  $4xCO_2$  consists of robust decreases in  
 62 the tropical lower stratosphere (LS), increases in the tropical upper stratosphere and in-  
 63 creases over high latitudes (Chiodo et al., 2018). While the exact details of these changes  
 64 are model dependent, especially over high latitudes, the general pattern is very consis-  
 65 tent among models (Nowack et al. (2015), Chiodo et al. (2018), Chiodo and Polvani (2019)  
 66 (hereafter CP2019)).

67 This pattern of reduced (increased) ozone over the tropical lower (high latitude)  
 68 LS in response to  $4xCO_2$  has immediate implications for temperature gradients in the  
 69 stratosphere by cooling the tropics and warming high latitudes (Nowack et al. (2015);  
 70 Chiodo et al. (2018)). As CP2019 showed, these changes in temperature gradients drive  
 71 an anomalous equatorward shift of the midlatitude jet, not only in the Southern Hemi-  
 72 sphere (SH), but also in the Northern Hemisphere (NH), where anomalies extend down

73 into the lower troposphere and are concentrated over the Atlantic, resembling the neg-  
74 ative phase of the North Atlantic Oscillation (NAO).

75 A more recent study by Zhang et al. (Submitted), that considered two models that  
76 differed only in their representation of interactive chemistry, also showed that changes  
77 in composition can impact the sign of the NH midlatitude jet response to increased CO<sub>2</sub>.  
78 However, in contrast to CP2019, the long-term impact of this compositional feedback  
79 was a *poleward*, not equatorward, shift in the North Atlantic jet. Though not investi-  
80 gated in detail, this poleward shift of the jet was linked to changes in the ocean circula-  
81 tion, which were not examined in CP2019. More precisely, Zhang et al. (Submitted)  
82 noted that the AMOC exhibited a stronger decline in the interactive versions of simu-  
83 lations in which trace gases and aerosols were allowed to respond to increased CO<sub>2</sub>, rel-  
84 ative to non-interactive simulations. Indeed, recent studies have highlighted the large  
85 influence that changes in the AMOC exert on the response of the NH midlatitude jet to  
86 increased CO<sub>2</sub> (Gervais et al. (2019)), with models featuring a larger AMOC decline also  
87 tending to produce a stronger poleward jet shift (Bellomo et al. (2021); Liu et al. (2020);  
88 Orbe et al. (Under Review)).

89 The results from Zhang et al. (Submitted) suggest that composition feedbacks on  
90 the NH midlatitude jet likely depend on the response of the ocean circulation. However,  
91 that study did not examine the mechanism underlying the stronger AMOC response in  
92 the interactive chemistry simulations nor did it isolate the role of ozone from influences  
93 due to other trace gases and aerosols. To this end, here we hypothesize that the ozone-  
94 induced negative NAO wind anomalies reported in CP2019 provide a potential pathway  
95 through which stratospheric ozone changes can influence the AMOC. Variations in the  
96 jet – namely those resembling the NAO – have long been shown to influence variabil-  
97 ity of the AMOC through changes in wind stress (Marshall et al. (2001); Zhai and Mar-  
98 shall (2014)). Modified air-sea fluxes of heat, water and momentum associated with vari-  
99 ations in the NAO alter vertical and horizontal density gradients in the subpolar gyre,  
100 inducing changes in deep water formation and the AMOC (e.g., Visbeck et al. (1998);  
101 Delworth and Dixon (2000)). This pathway via the NAO has been used to demonstrate  
102 how sudden stratospheric warmings influence the variability of heat flux anomalies into  
103 the ocean and ocean mixed layer depths in the North Atlantic (O’Callaghan and Mitchell  
104 (2014)) as well as the strength of the AMOC itself (Reichler et al. (2012)).

105 We begin by showing results from non-interactive and fully interactive chemistry  
106 global warming experiments produced with the new high-top coupled atmosphere ocean  
107 version of the NASA Goddard Institute for Space Studies (GISS) climate model that were  
108 submitted to the Coupled Model Intercomparison Project Phase 6 (CMIP6) (Eyring et  
109 al. (2016)). We then show that the AMOC response in the interactive simulations is largely  
110 associated with changes in stratospheric ozone, not aerosols, using new experiments in  
111 which the stratospheric ozone response to 4xCO<sub>2</sub> is isolated from changes in other trace  
112 gases and aerosols. In particular, we show that our model captures the ozone-induced  
113 negative NAO-like pattern first reported in CP2019; in addition, we also find that ozone-  
114 driven changes in surface friction speed further weakens the AMOC, resulting in a long-  
115 term poleward shift of the NH jet. As a result, we show that both stratospheric ozone  
116 changes and the AMOC influence the NH jet on distinct “fast” and “long” timescales  
117 (and in the opposite sense), comprising a coupled atmosphere-ocean feedback on the NH  
118 midlatitude jet response to increased CO<sub>2</sub>. While the former “fast” feedback was doc-  
119 umented in CP2019, the latter has, to the best of knowledge, not been reported in pre-  
120 vious studies.

121 It is important to note that previous studies have long shown that interactive at-  
122 mospheric composition can strongly influence the AMOC, placing an almost exclusive  
123 focus on the role of aerosols (Booth et al., 2012; Cowan & Cai, 2013; Swingedouw et al.,  
124 2015). More recently, Rind et al. (2018) also identified a larger sensitivity of the AMOC  
125 response to global warming using an interactive configuration of the CMIP5 version of

126 the GISS climate model (GISS-E2-R), compared to a non-interactive version. In that  
 127 study, multicentennial cessations of the AMOC were found to occur in simulations in which  
 128 natural aerosols (primarily sea salt) were allowed to locally cool sea surface temperatures  
 129 through their influence on cloud optical thickness; these cooler SSTs were then linked  
 130 to reduced evaporation relative to precipitation, resulting in positive surface freshwater  
 131 forcing and reduced NADW production. As in Rind et al. (2018) we also show that com-  
 132 positional feedbacks play an important role on the response of the AMOC to CO<sub>2</sub> through  
 133 their influence on surface fluxes and surface temperatures. However, the mechanism pro-  
 134 posed here only invokes changes in stratospheric ozone, not aerosols.

135 We begin by discussing methods in Section 2 and present key results and conclu-  
 136 sions in Sections 3 and 4, respectively.

## 137 2 Methods

### 138 2.1 Model and Configurations

139 Here we use the NASA Goddard Institute for Space Studies (GISS) “Middle At-  
 140 mosphere (MA)” Model E2.2 (Rind et al. (2020); Orbe et al. (2020)). E2.2 consists of  
 141 102 vertical levels spanning the surface up to 0.002 hPa and is run at a horizontal res-  
 142 olution of 2 degrees by 2.5 degrees. Orographic and non-orographic gravity wave drag  
 143 is parameterized following Lindzen (1987) and Rind et al. (1988), producing in E2.2 a  
 144 quasibiennial oscillation (QBO) that compares well with observations as well as improved  
 145 stratospheric polar vortex variability (Ayarzagüena et al. (2020); Rind et al. (2020)). Among  
 146 the different model versions discussed in Rind et al. (2020) here we focus on the “Altered-  
 147 Physics” (-AP) Version (E2.2-AP) because this is the configuration that was submitted  
 148 CMIP6 and presented in recent studies (Ayarzagüena et al. (2020); DallaSanta et al. (2021a,  
 149 2021b)).

150 We begin by showing the results reported in Zhang et al. (Submitted) using both  
 151 “Non-INTeractive” (NINT) (Table 1, row 1-3) and fully interactive OMA (“One-Moment  
 152 Aerosols”; Bauer et al. (2020)) configurations (Table 1, row 4-6). In the NINT config-  
 153 uration (denoted in CMIP6 as “physics version 1” on the Earth System Grid Federation  
 154 (ESGF; <https://esgf.llnl.gov>)) all trace gases and aerosols are set to preindustrial val-  
 155 ues. Hence, in the 2- and 4xCO<sub>2</sub> NINT runs neither ozone nor other trace gases (besides  
 156 water vapor) change in response to increased CO<sub>2</sub>. By comparison, the OMA 2- and 4xCO<sub>2</sub>  
 157 runs (denoted in CMIP6 as “physics version 3” on ESGF) capture the full nonlinear ozone  
 158 response to CO<sub>2</sub>, as well as composition feedbacks associated with other trace gases and  
 159 aerosols.

160 In order to isolate the role of ozone feedbacks on the circulations, we then use a  
 161 linearized ozone (LINOZ) configuration (Table 1, row 7-8). In LINOZ (McLinden et al.  
 162 (2000)) the ozone field is calculated interactively by Taylor expanding the equation of  
 163 state around present-day (2000–2010) values such that the ozone tendency is, to first-  
 164 order, parameterized as a function of the local ozone mixing ratio, temperature, and over-  
 165 head column ozone. Tropospheric ozone is calculated using monthly mean ozone pro-  
 166 duction and loss rates archived from GEOS-CHEM (Rind et al. (2014)). In contrast to  
 167 NINT, therefore, the LINOZ ensemble captures the influence of the ozone response to  
 168 CO<sub>2</sub> on the large-scale circulation. Unlike OMA, however, it is much more computationally  
 169 efficient to run and isolates the ozone feedback from feedbacks related to other trace  
 170 gases and aerosols. DallaSanta et al. (2021a) previously showed that the LINOZ ozone  
 171 parameterization reproduces well the vertical structure and seasonal cycle of stratospheric  
 172 ozone obtained from the fully interactive OMA configuration (see their Figure 1).

**Table 1.** The Model E2.2 experiments presented in this study, including preindustrial control, abrupt 2xCO<sub>2</sub> and abrupt 4xCO<sub>2</sub> simulations using both NINT (rows 1-3) and OMA (rows 4-6) configurations. Four NINT abrupt 4xCO<sub>2</sub> ensemble members are included (row 3) in order to compare with a four member 4xCO<sub>2</sub> ensemble produced using the LINOZ configuration (row 8). The 4xCO<sub>2</sub> ensemble mean LINOZ ozone response is also used to force four AMIP preindustrial experiments (row 9) in which all forcings other than ozone are set to preindustrial values. A LINOZ preindustrial control simulation (row 7) is also examined. All coupled simulations are run using the the GISS Ocean v1 (GO1) (i.e., “-G” in CMIP6 notation).

Configuration	Ozone	CO <sub>2</sub>	Ensemble Size	SSTs and SICs
NINT	Preindustrial	Preindustrial	1	coupled (-G ocean)
NINT	Preindustrial	2xCO <sub>2</sub>	1	coupled (-G ocean)
NINT	Preindustrial	4xCO <sub>2</sub>	4	coupled (-G ocean)
OMA	Preindustrial	Preindustrial	1	coupled (-G ocean)
OMA	2xCO <sub>2</sub>	2xCO <sub>2</sub>	1	coupled (-G ocean)
OMA	4xCO <sub>2</sub>	4xCO <sub>2</sub>	1	coupled (-G ocean)
LINOZ	Preindustrial	Preindustrial	1	coupled (-G ocean)
LINOZ	4xCO <sub>2</sub>	4xCO <sub>2</sub>	4	coupled (-G ocean)
NINT	LINOZ 4xCO <sub>2</sub>	Preindustrial	4	AMIP (PiControl SSTs and SICs)

173

## 2.2 Experiments

174

175

176

177

178

179

180

181

182

183

184

For the different model configurations (NINT, OMA, LINOZ) we perform 150-year-long abrupt 2- and 4xCO<sub>2</sub> experiments, in which CO<sub>2</sub> values are abruptly doubled and quadrupled relative to preindustrial values. For each model configuration, these experiments are branched from a corresponding preindustrial control simulation. For NINT and LINOZ four-member 4xCO<sub>2</sub> ensembles are run in order to assess the robustness of any ozone feedbacks. These experiments are all conducted using the coupled-atmosphere-ocean version of E2.2-AP coupled to the GISS Ocean v1 (GO1) (i.e., “-G” in CMIP6 notation, hereafter simply E2-2-G). For coupled atmosphere-ocean configurations in which (four-member) ensembles are run, different ensemble members are chosen from different initial ocean states spaced 20 years apart in the corresponding preindustrial control simulation.

185

186

187

188

189

190

191

192

In addition to the coupled atmosphere-ocean experiments, we also present results from a four-member ensemble of 60-year-long atmosphere-only AMIP experiments in which sea surface temperatures (SSTs) and sea ice concentrations (SICs) are fixed to preindustrial values, but the monthly mean time-evolving ensemble mean ozone response from the coupled LINOZ 4xCO<sub>2</sub> experiments is prescribed (Table 1, row 9). This allows us to quantify the impact of the ozone feedback represented in LINOZ on the large-scale circulation, absent any contributions from changes in background CO<sub>2</sub>, sea ice concentrations or sea surface temperatures.

193

## 2.3 Analysis

194

### 2.3.1 Timescales

195

196

197

When examining the midlatitude jet response to increased CO<sub>2</sub> we account for the fact that extratropical circulation changes consist of distinct “fast” and “slow” responses (Ceppi et al. (2018), hereafter CZS2018). More precisely, CZS2018 show that most of

198 the shift of the midlatitude jets occurs within 5-10 years of a steplike (abrupt) CO<sub>2</sub> forc-  
 199 ing, with little shifts occurring during a slower response over which SSTs change over  
 200 subsequent decades. In contrast to the Southern Hemisphere, zonal asymmetries play  
 201 an important role in the Northern Hemisphere, where the influence of local patterns in  
 202 sea surface temperature change can result in oppositely signed jet shifts on “slow” timescales.

203 Given the potential for compensating jet shifts occurring on distinct timescales, we  
 204 decompose the CO<sub>2</sub> circulation response into “fast” and “long” timescale responses. This  
 205 consideration is especially important as it relates to our hypothesis that stratospheric  
 206 ozone changes can first result in an initial equatorward shift of the jet (CP2019) but, over  
 207 time, result in a poleward shift of the jet via their influence on the AMOC (Bellomo et  
 208 al., 2021; Orbe et al., Under Review).

209 In order to account for the large internal variability in our runs, perhaps related  
 210 to a somewhat larger ENSO amplitude in our model compared to observations (Rind et  
 211 al. (2020)), we modify the original approach used in CZS2018 to define our “fast” response  
 212 as the difference between the ensemble mean 4xCO<sub>2</sub> response, averaged over years 5-20  
 213 (as opposed to years 5-10), and the corresponding preindustrial control simulation. In  
 214 addition, instead of focusing on the “slow” response, defined in that study as the differ-  
 215 ence between averages over years 120-140 and years 5-10, here we examine the “long”  
 216 response, defined as the difference between the ensemble mean 4xCO<sub>2</sub> response, aver-  
 217 aged over years 100-150, and the preindustrial control simulation. While this definition  
 218 departs from the approach used in CZS2018, it is more consistent with the Zhang et al.  
 219 (Submitted) and CP2019 studies motivating our study, with which we directly compare  
 220 our results throughout. Note that in response to an abrupt quadrupling of CO<sub>2</sub> the NINT  
 221 model configuration produces global mean surface temperature “fast” and “long” responses  
 222 of  $\sim 2.9^\circ\text{C}$  and  $\sim 3.9^\circ\text{C}$ , respectively. Statistical significance of all changes are assessed  
 223 relative to the interannual variability in the corresponding preindustrial control simu-  
 224 lation for each configuration (Table 1, rows 1,4,7).

### 2.3.2 Analysis Fields

226 In addition to the atmospheric variables examined in CP2019 (i.e., zonal mean wind,  
 227 zonal mean temperature, surface temperature, 850 hPa zonal wind) we examine ocean  
 228 variables relevant to understanding the evolution of the AMOC and its coupling to the  
 229 atmosphere. In particular, in addition to examining the surface mixed layer depths we  
 230 also examine sea surface temperatures, surface friction speed, horizontal ocean heat and  
 231 salinity transports as well as the net heat fluxes which, together with the net freshwa-  
 232 ter fluxes,  $F$  (inferred from precipitation minus evaporation (P-E)), provide information  
 233 about the surface buoyancy forcing (Large and Yeager (2009)). In our simulations, the  
 234 preindustrial climatological buoyancy forcing over the North Atlantic is dominated by  
 235 the net heat fluxes ( $Q = Q_H + Q_E + Q_S + Q_L$ ), which are defined to be positive into the  
 236 ocean (Appendix Figure 1, left). These are further partitioned into their respective la-  
 237 tent heat ( $Q_E$ ) and sensible heat ( $Q_H$ ) contributions as we find that the net solar ( $Q_S$ )  
 238 and longwave ( $Q_L$ ) flux radiative contributions are negligible over the North Atlantic re-  
 239 gion (Appendix Figure 1, right).

240 Given our interest in the Northern Hemisphere we focus primarily on December-  
 241 January-February (DJF). The ocean heat transport changes in our simulations are also  
 242 most pronounced during DJF, consistent with the analyses presented in Romanou et al.  
 243 (Under Review) and Orbe et al. (Under Review).

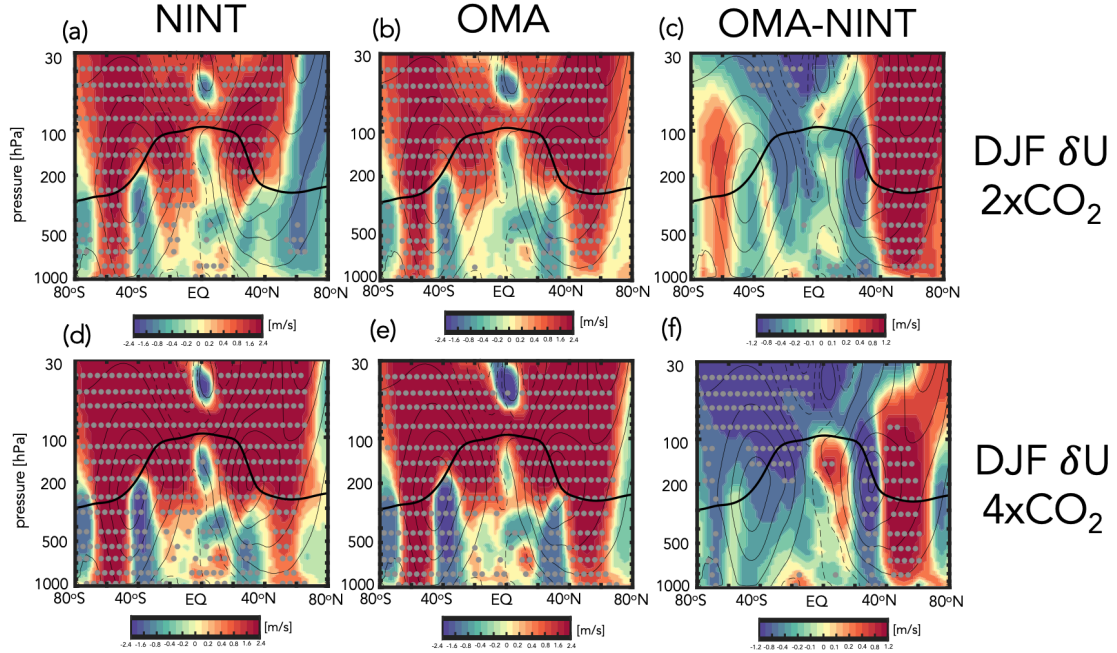


**Figure 1.** Colors show the December-January-February (DJF) response of the zonal mean zonal winds,  $U$ , to an abrupt doubling (top) and quadrupling (bottom) of  $\text{CO}_2$ , averaged over years 100-150. Results are shown for the “Non-INteractive” (NINT) (a,d) and fully interactive OMA (“One-Moment Aerosols”) configurations (b,e), where one ensemble member has been used for each forcing scenario. The OMA - NINT differences are also shown (c,f). Black contours denote climatological mean DJF  $U$  values (contour interval: 8 m/s). Stippled regions are statistically significant and the black thick line shows the climatological mean tropopause in the preindustrial control NINT simulation. Note that all colorbar bounds are consistent with those used in Chiodo and Polvani (2019) in order to facilitate comparisons with that study.

244 **3 Results**

245 **3.1 Abrupt  $2\times\text{CO}_2$  and  $4\times\text{CO}_2$  Zonal Mean Wind Response: OMA versus NINT**

246

247 Before focusing on ozone feedbacks, we first review the OMA versus NINT differ-  
 248 ences in NH jet behavior that were presented in Zhang et al. (Submitted) (Figure 1). In  
 249 the stratosphere the zonally averaged DJF wind response to 2- and  $4\times\text{CO}_2$  features an  
 250 acceleration at nearly all latitudes, consistent with amplified warming in the tropical upper  
 251 troposphere (T. A. Shaw (2019)) and increased cooling of the stratosphere with height  
 252 (Garcia and Randel (2008)). Similar wind responses emerge in both the NINT and OMA  
 253 configurations, except over northern high latitudes at  $2\times\text{CO}_2$ , where the differences in  
 254 NINT are not statistically significant.

255 In the troposphere, however, there are noticeable differences between the OMA and  
 256 NINT simulations. In particular, the NH midlatitude jet features a much stronger pole-  
 257 ward shift in OMA, compared to NINT (Figures 3 and 6 in Zhang et al. (Submitted) for  
 258 comparison). As discussed in that study, the stronger response in OMA results in en-  
 259 hanced eddy mixing along isentropes on the poleward flank of the NH jet, resulting in  
 260 increased transport of tracers from the northern midlatitude surface to the Arctic (not  
 261 shown). This difference between OMA and NINT occurs at both 2- and at  $4\times\text{CO}_2$ , re-

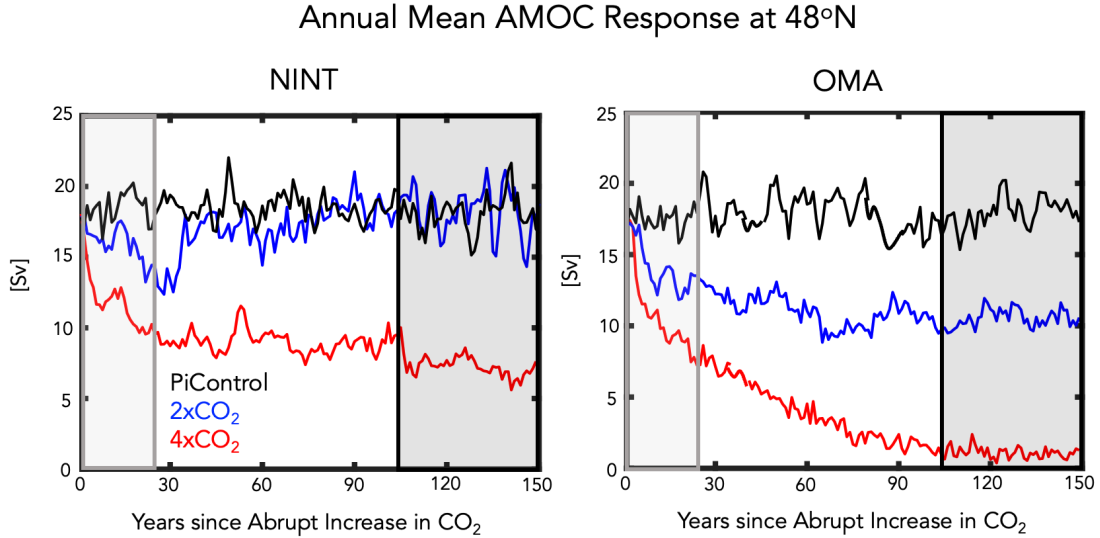


**Figure 2.** Changes in the annual mean maximum overturning stream function in the Atlantic ocean, evaluated 48°N, for the preindustrial control (black), abrupt 2xCO<sub>2</sub> (blue) and abrupt 4xCO<sub>2</sub> (red) simulations. Results for the NINT (left) and OMA (right) configurations are shown. Black and grey shaded boxes denote the “fast” and “long” timescale response averaging periods.

262 sulting in a nonlinearity in the jet (and tracer transport) response in NINT that is not  
 263 present in the OMA simulations. In the SH, by comparison, the differences between OMA  
 264 and NINT are much smaller and not statistically significant.

265 Zhang et al. (Submitted) showed that the nonlinearity in NH jet behavior evident  
 266 in the “long” response in the NINT model configuration was related to a nonlinear AMOC  
 267 response to CO<sub>2</sub> forcing (Figure 2). That is, despite an initial weakening, in response  
 268 to 2xCO<sub>2</sub>, the AMOC eventually recovers in the NINT 2xCO<sub>2</sub> simulation to preindus-  
 269 trial values, in contrast to the response to 4xCO<sub>2</sub> in which the AMOC is about 10 SV  
 270 weaker than the preindustrial control (black boxes). This results in a so-called “AMOC  
 271 nonlinearity” of  $\sim 5$ SV in the NINT configuration. By comparison, in the OMA config-  
 272 uration, the AMOC weakens by  $\sim 7$  and  $\sim 17$  SV in the 2- and 4xCO<sub>2</sub> simulations, re-  
 273 spectively, representing only a very weak nonlinearity in the AMOC (of  $\sim 1.5$  SV).

274 As it is difficult to meaningfully interpret the zonal mean wind response in the NH,  
 275 where there are large zonal variations in the midlatitude jet (Simpson et al. (2014)), we  
 276 next compare the 850 hPa zonal wind changes between the NINT and OMA 4xCO<sub>2</sub> sim-  
 277 ulations, further distinguishing between “fast” and “long” responses (Figure 3). We be-  
 278 gin with the NINT equilibrated or “long” response (i.e. years 100-150), which consists  
 279 of a poleward jet shift over the Pacific basin and an acceleration and eastward extension  
 280 of the jet over the Atlantic (Fig. 3b). This pattern is amplified in the OMA run (Fig.  
 281 3d), in which both the strengthening of the jet over the Atlantic and its poleward shift  
 282 over the Pacific are more pronounced. This wind response in OMA, relative to NINT,  
 283 is consistent with the jet differences identified in Orbe et al. (Under Review) between  
 284 two non-interactive simulations of the GISS low-top climate model in which only the AMOC  
 285 strength differed. This suggests that the jet differences between OMA and NINT on these  
 286 longer timescales are primarily driven by differences in the AMOC response, as concluded  
 287 in Zhang et al. (Submitted).



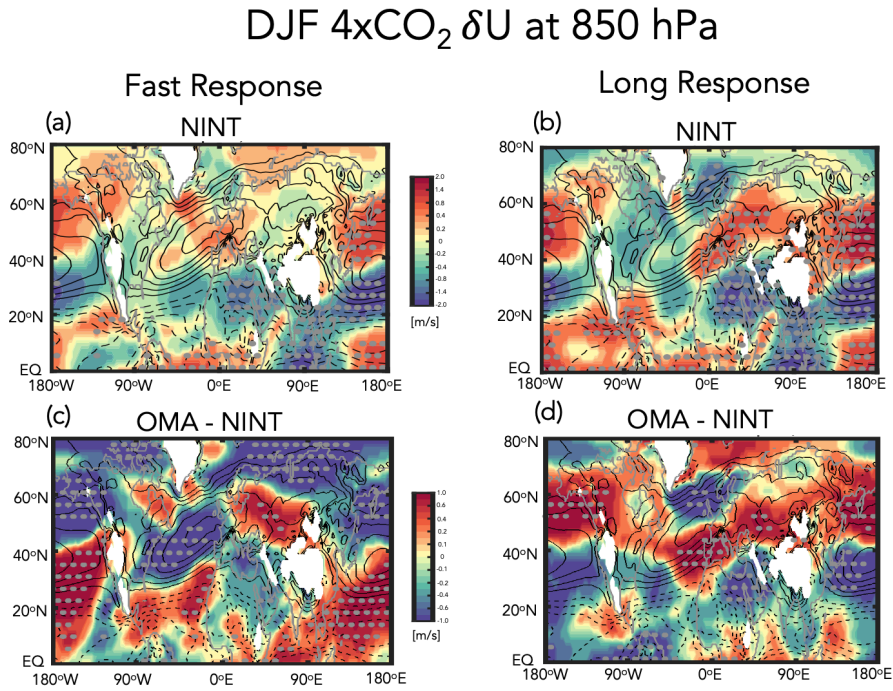


**Figure 3.** Colors show the  $4\times\text{CO}_2$  (four member) ensemble mean change in the DJF 850 hPa zonal winds for the NINT configuration, decomposed into “fast” (i.e. years 5-20) (a) and “long” (i.e. years 100-150) (b) responses. The OMA - NINT fast and long differences are shown in (c) and (d), respectively. Note that one ensemble member is used in displaying the OMA - NINT differences. Black contours denote climatological mean DJF values ( $U$  contour interval: 2 m/s) and stippled regions are statistically significant.

Figure 2 (grey boxes) highlights how the AMOC differences between OMA and NINT noted in Zhang et al. (Submitted) arise very early in the simulations (within the first 20 years). Over these years – which comprise the “fast” response – the impact of interactive chemistry on the zonal wind changes is very different (Fig. 3a,c). In particular, over the Atlantic, interactive composition results in a strong weakening over the jet core and an acceleration on the equatorward flank of the jet (Fig. 3c). The jet response is also very different over the Pacific, where the jet shifts equatorward, not poleward as in the NINT simulation (Fig. 3a).

This fast composition feedback that occurs over years 5-20 is consistent with the results from CP2019, who showed that the ozone response to 4xCO<sub>2</sub> induces a weakening of the North Atlantic jet and a strengthening on its equatorward flank (see their Figure 6). This response is reminiscent of the negative phase of the NAO which previous studies have shown can result in a weaker AMOC Delworth and Zeng (2016). In CP2019, however, this response is realized through changes in stratospheric ozone alone, whereas in OMA all trace gases and aerosols are responding. Furthermore, the significance of this rapid response with only one ensemble member is uncertain, particularly during the first 5-20 years when the signal is confounded by large internal variability. To this end, next we present results from the larger (4-member) LINOZ ensemble to examine whether the fast response in the NH jet is related to stratospheric ozone changes.

### 3.2 Abrupt 4xCO<sub>2</sub> Stratospheric Ozone and Temperature Responses: OMA versus LINOZ

Before examining the circulation response in the LINOZ ensemble, we first compare the annually averaged ensemble mean LINOZ 4xCO<sub>2</sub> ozone response with that from the OMA simulation (Figure 4). The amplitude and pattern of the ozone response in the LINOZ ensemble (Fig. 4b) is generally very similar to the ozone response in the OMA simulation (Fig. 4a). In both configurations the pattern of the 4xCO<sub>2</sub> changes reflects a decrease in tropical LS ozone, associated with enhanced tropical upwelling (Garcia and Randel (2008)), and enhanced concentrations over high latitudes. Over all latitudes the ozone changes are statistically significant, relative to interannual variability in the preindustrial control simulation.

Over northern high latitudes there are some differences in the mid-to-lower stratosphere (~30-100 hPa) between LINOZ and OMA, generally consistent with Chiodo et al. (2018), who found that in this region the ozone response to CO<sub>2</sub> is somewhat more model dependent. Furthermore, both simulations feature small changes in the troposphere. Overall, therefore, the LINOZ scheme captures the gross characteristics of the ozone abrupt 4xCO<sub>2</sub> response expected from previous studies. Note that this ozone response occurs in both simulations within the 5-20 years that comprise the “fast” response timescale, although full equilibration at high latitudes does take somewhat longer (not shown).

In response to the ozone changes to 4xCO<sub>2</sub> both the OMA simulation and LINOZ ensemble produce cooling in the tropical lower stratosphere and warming over high latitudes (Fig. 4c,d). The amplitude of the cooling is ~3K in the tropical lower stratosphere, and is more-or-less collocated with the region of largest ozone decreases. Further analysis of the temperature tendencies reveals that in our model the cooler temperatures in the tropics (20°S-20°N) and high latitudes (40°N) are respectively associated with reduced and increased radiative heating, primarily in the shortwave component (not shown). Dynamically, comparisons of the 4xCO<sub>2</sub> changes in the residual mean stream function show a weaker response in LINOZ, relative to NINT (Appendix Figure 2). This ozone feedback on the Brewer-Dobson circulation, first identified in (DallaSanta et al., 2021a), would contribute to reduced upwelling (and adiabatic cooling) and ozone transport within the lower tropical stratosphere. These circulation changes are therefore not the primary

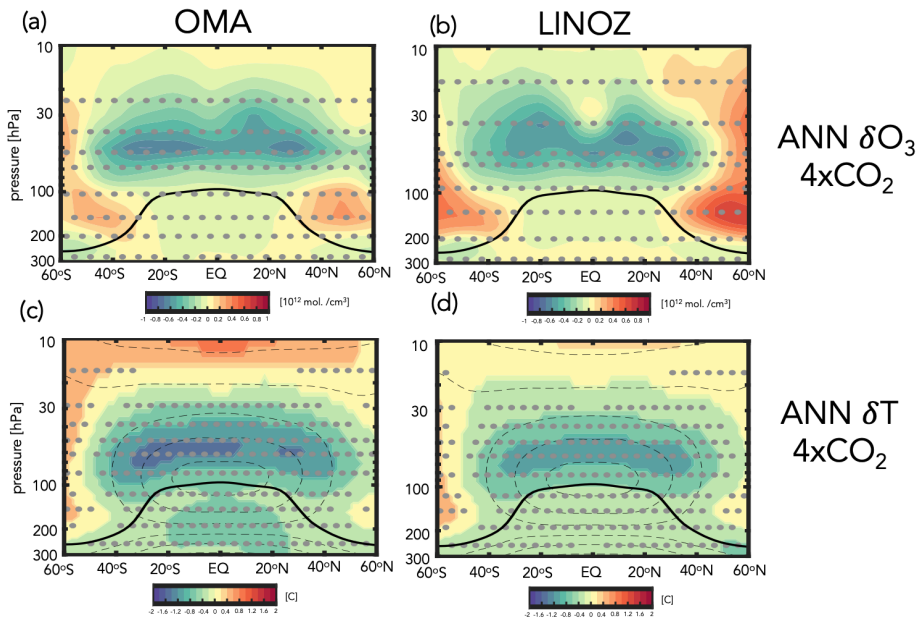


**Figure 4.** Colors show the annual averaged change in ozone number density (top) and temperature (bottom) in response to  $4xCO_2$ . Results for OMA (left) and LINOZ (right) are shown, averaged over years 5-20. One simulation is shown for OMA and the four-member ensemble mean response is shown for LINOZ. Black contours in the bottom panels show climatological mean temperatures (contour interval: 10 C). Stippled regions are statistically significant and the black thick line shows the climatological mean tropopause in the preindustrial control NINT simulation.

338 drivers of the temperature response which, rather, is primarily determined by the short-  
 339 wave radiative response to ozone changes.

340 Despite the somewhat stronger cooling in OMA (Fig. 4c) compared to NINT (Fig.  
 341 4d), the temperature response in both configurations is within the 2-4 K range documented  
 342 in CP2019 (note that all colorbars used are consistent with that study to facilitate compar-  
 343 isons with their results). As the authors of that study emphasized, the temperature  
 344 changes due to ozone are of a similar magnitude to the temperature changes due to 4xCO<sub>2</sub>  
 345 alone in the tropical lower stratosphere (i.e., considering no ozone feedback), where the  
 346 stratosphere cools by ~2K in the NINT ensemble (not shown). The ozone changes present  
 347 in LINOZ (and OMA) therefore represent a substantial feedback on the CO<sub>2</sub>-induced  
 348 cooling in the stratosphere.

### 349 **3.3 Ozone Feedback on Northern Hemisphere Jet: Fast Response**

350 The temperature response due to ozone is dynamically consequential for the tropo-  
 351 sphere to the extent that it modifies temperature gradients (and winds) in the lower  
 352 stratosphere. Indeed, the LINOZ ensemble shows a strong enhancement of lower strato-  
 353 spheric temperature gradients in both hemispheres on both the fast and long response  
 354 timescales (Fig. 5a,b). In the fast response, which we focus on first, this reduction in the  
 355 meridional temperature gradient near the tropopause has important consequences for  
 356 the midlatitude jet in both hemispheres, which strengthens above and along the jet core  
 357 and weakens on the poleward flank of the jet over latitudes north of ~ 50°N (Fig. 5c).  
 358 The winds also accelerate equatorward of the jet core, relative to NINT, in both hemi-  
 359 spheres, although the response is only statistically significant in our model in the NH.  
 360 This ozone-induced response in the jet is very similar to the pattern of the wind response  
 361 reported in CP2019 (see their Figures 4 and 5). As with the temperature changes occur-  
 362 ring in the lower stratosphere, the wind response to ozone changes is similar in mag-  
 363 nitude to the 4xCO<sub>2</sub> response, again suggesting a substantial modulation of the circula-  
 364 tion in both hemispheres by ozone changes alone.

365 The fast zonal mean response to ozone changes reflects a weakening of the polar  
 366 jet over all longitudes, with the largest negative anomalies concentrated over the Atlantic  
 367 ocean that are flanked equatorward by positive wind anomalies (Fig. 6a). These wind  
 368 changes are vertically coherent throughout the troposphere as the LINOZ-NINT changes  
 369 are similar at 300 hPa (not shown). This LINOZ-NINT wind dipole over the Atlantic  
 370 is very similar to the fast wind response captured in the fully interactive OMA simula-  
 371 tion (Fig. 3c), especially over the Atlantic. Over the Pacific, by comparison, the OMA  
 372 and LINOZ responses are different, consistent with CP2019 who found no robust ozone  
 373 feedback over the Pacific (see their Figure 5). Furthermore, the weakening of the North  
 374 Atlantic jet in the LINOZ simulations is associated with warming over North America  
 375 and cooling over the North Atlantic and over Eurasia, resembling the negative phase of  
 376 the NAO (Fig. 6c). A similar surface temperature anomaly was identified in CP2019 (see  
 377 their Figure 7) in conjunction with positive sea level pressure (SLP) anomalies over the  
 378 Arctic, both features being reminiscent of a negative NAO (Appendix Figure 3, top).

### 379 **3.4 Ozone Feedback on Northern Hemisphere Jet: Long Response**

380 Interestingly, while the fast responses in the winds and temperatures in the LINOZ  
 381 ensemble are highly consistent with the results from CP2019, our model also simulates  
 382 a distinct “long” response characterized by strong cooling over the Arctic from the sur-  
 383 face to the mid-to-upper troposphere (Fig. 5b). This cooling, which was not identified  
 384 in CP2019, results in enhanced mid-to-lower tropospheric temperature gradients, prompt-  
 385 ing a strong poleward shift of the NH jet and a statistically significant acceleration of  
 386 the winds at 50°N exceeding 2 m/s (Fig. 5d).

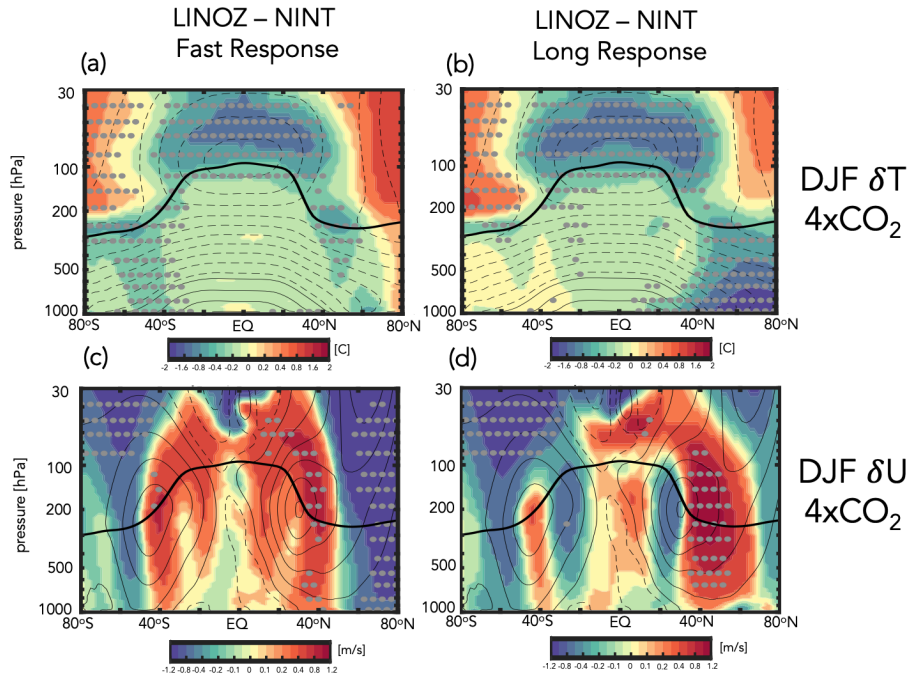


**Figure 5.** Colors show the LINOZ-NINT ensemble mean difference in the DJF response of the zonal mean temperatures,  $T$  (top) and zonal winds,  $U$  (bottom) in response to an abrupt quadrupling of  $\text{CO}_2$ . Both LINOZ and NINT ensembles consist of four members. Responses are decomposed into “fast” (a,c) and “long” (b,d) changes. Contours denote climatological mean DJF values ( $T$  contour interval: 10 C;  $U$  contour interval: 8 m/s). Stippled regions are statistically significant and the black thick line shows the climatological mean tropopause in the preindustrial control simulation.

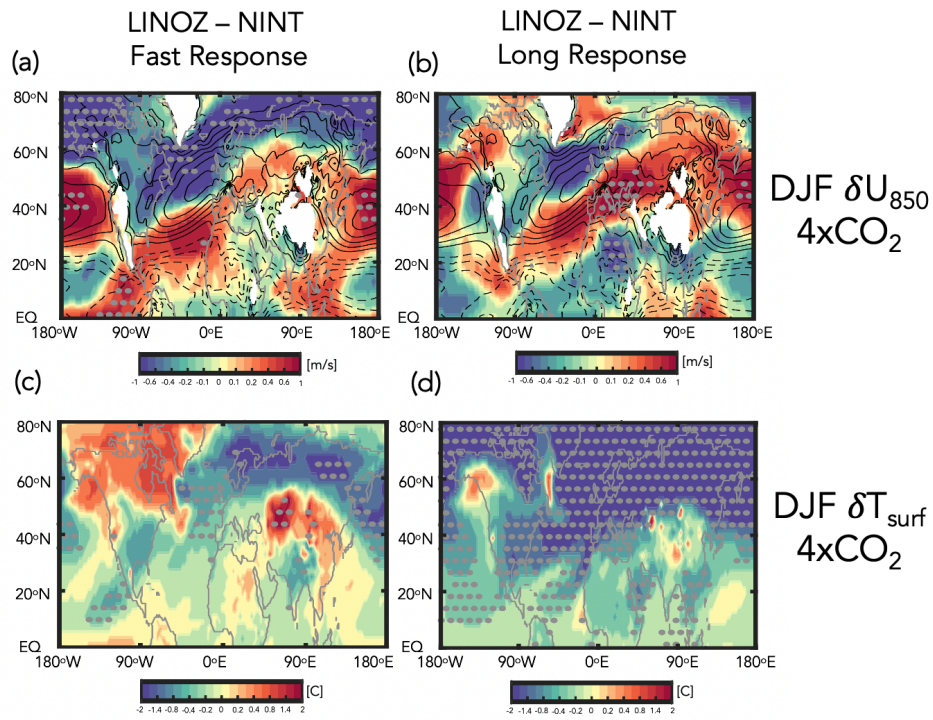


**Figure 6.** Same as Figure 5, except showing the LINOZ-NINT DJF response in the 850 hPa zonal winds,  $U_{850}$  (top) and surface temperatures,  $T_{\text{surf}}$  (bottom). Contours in top panels denote climatological mean DJF values of  $U_{850}$  (contour interval: 2 m/s). Note the similarity between the “fast” wind response shown in (a) and the CP2019 results (their Figure 6).

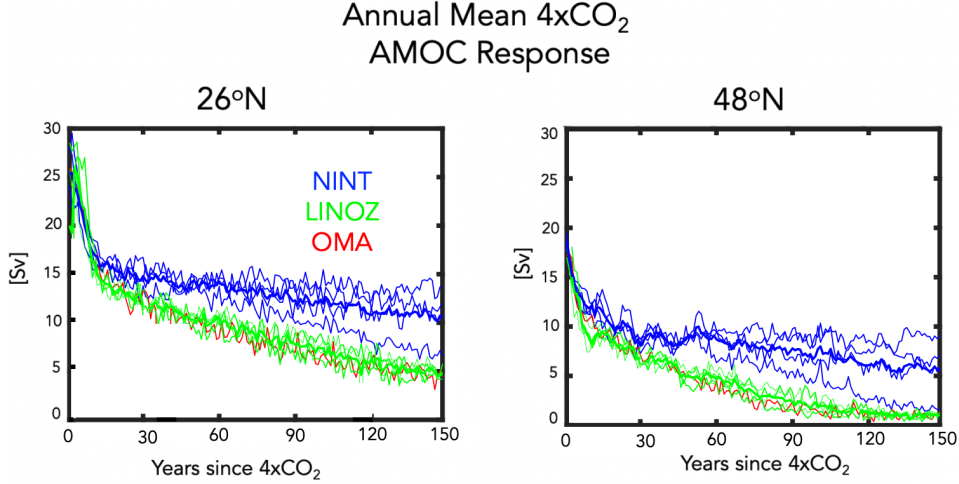


**Figure 7.** Changes in the annual mean maximum overturning stream function in the Atlantic ocean, evaluated at 26°N (left) and 48°N (right) in response to 4xCO<sub>2</sub>, relative to the preindustrial control simulations. Results for the LINOZ and NINT ensembles are shown in green and blue, respectively (thick lines denote ensemble means). Red lines show the response in the OMA simulation.

387 Zonally, the cooling over the Arctic occurring in the LINOZ ensemble during the  
 388 long response primarily reflects hemispheric-wide cooling over the Arctic associated with  
 389 an expansion of the North Atlantic Warming Hole (Fig. 6d). This enhancement of merid-  
 390 ional temperature gradients in the lower and mid troposphere drives a poleward shift that  
 391 spans all longitudes and originates over the North Atlantic (Fig. 6b), where the jet ex-  
 392 hibits a distinct acceleration and eastward extension over Europe. Note that over the  
 393 jet core (40-50°N) the winds accelerate (in the zonal mean) during both “fast” (Fig. 5c)  
 394 and “long” responses (Fig. 5d). However, north of 50°N the responses are very differ-  
 395 ent, with the fast response exhibiting a strong weakening, in contrast to the accelera-  
 396 tion occurring on longer (i.e., “long” response) timescales. This behavior north of 50°N  
 397 was not captured in CP2019 and comprises an ozone feedback that is distinct from what  
 398 was outlined in that study.

399 **3.5 Long Ozone Feedback: Modulation by the AMOC**

400 The “long” responses in the tropospheric winds and temperatures that occurs in  
 401 the LINOZ ensemble are not obviously linked to ozone-driven temperature changes in  
 402 the stratosphere, which do not extend into the troposphere. What, then, is the driver  
 403 of the lower tropospheric high latitude cooling, if it is not directly linked to ozone-driven  
 404 stratospheric temperature changes?

405 As expected from the OMA and NINT results presented in Zhang et al. (Submitted),  
 406 we find that the strong cooling that occurs over the NH in the long LINOZ response  
 407 is also related to a weakening of the AMOC at 4xCO<sub>2</sub> (Mitevski et al. (2021); Rind et  
 408 al. (2020); Orbe et al. (Under Review)). In particular, Figure 7 shows stronger weaken-  
 409 ing of the AMOC in the LINOZ (green lines) ensemble, relative to NINT (blue lines) at  
 410 both 26°N (left) and at 48°N (right). Despite large internal variability, the LINOZ en-  
 411 semble shows a more rapid decline of the AMOC, a difference that is evident at both lat-  
 412 itudes.

413 Interestingly, comparisons of the AMOC behavior in LINOZ with the fully inter-  
 414 active OMA simulation (red line) shows a striking similarity (and the mechanism of these  
 415 changes is also similar, as shown in Section 3.6). This similarity is surprising, given that  
 416 other (non-ozone) trace gases and aerosols are also evolving in the OMA experiment. In  
 417 particular, Rind et al. (2018), using a previous version of the model, observed an indi-  
 418 rect effect of natural aerosols (primarily sea salt) on AMOC stability. They showed that  
 419 aerosols enhanced the local cooling of SSTs in regions of increased cloud cover in a warmer  
 420 climate by acting as condensation nuclei and thereby raising cloud optical thickness and  
 421 ocean surface cooling. This surface cooling was then linked to reduced evaporation rel-  
 422 ative to precipitation, resulting in anomalously positive surface freshwater forcing and  
 423 reduced North Atlantic Deep Water (NADW) production. That study, however, focused  
 424 on aerosol-induced AMOC cessations occurring on multicentennial timescales long af-  
 425 ter the initial (abrupt) warming. By comparison, the results in Figure 7 identify an im-  
 426 pact of ozone on the AMOC that occurs within the first 20 years of the initial CO<sub>2</sub> forc-  
 427 ing – that is, over the period during which stratospheric temperature gradients are most  
 428 impacted by ozone (not aerosols). Our results, therefore, highlight that during this time  
 429 frame the AMOC can be as (if not more) sensitive to wind-driven buoyancy changes forced  
 430 by stratospheric ozone anomalies as they are to aerosol-induced changes in freshwater  
 431 forcing.

432 Before elucidating the mechanism of the AMOC changes in the LINOZ ensemble,  
 433 we first identify the region over which the largest differences in mixed layer depth be-  
 434 gin to emerge between the LINOZ (OMA) and NINT simulations. In particular, the weaker  
 435 AMOC in the LINOZ and OMA runs is found to be accompanied by a rapid reduction  
 436 in mixed layer depths, which occur primarily in the Irminger Sea region (55°N-65°N,  
 437 40°W-20°W) (Figure 8). The mixed layer depth differences in the Labrador Sea are, by com-  
 438 parison, negligible. East of the Irminger Sea (i.e., 55°N–65°N, 20°W-0°) we also iden-  
 439 tify differences between the ensembles (not shown), but these emerge later, suggesting  
 440 that the Irminger Sea changes are likely the initiators of the differences in AMOC be-  
 441 havior between the NINT and LINOZ ensembles. A similar region was identified in Romanou  
 442 et al. (Under Review) as being key for determining the sensitivity of the AMOC, albeit  
 443 for the low-top model results and SSP 2-4.5 scenario considered in that study.

### 444 **3.6 Ozone Feedback Dependence on the AMOC: Linking Fast and Long** 445 **Responses**

446 Is the fact that the AMOC declines more rapidly in the LINOZ ensemble – and the  
 447 OMA run – a response to the ozone changes in those simulations or just a random oc-  
 448 currence? In the fast response the zonal wind changes over the North Atlantic reflect a  
 449 weakening of the jet core that is flanked equatorward by positive anomalies, resembling  
 450 a negative NAO pattern. Indeed, a negative (positive) NAO has been associated with  
 451 a weaker (stronger) AMOC by adding (extracting) heat to/from the subpolar gyre, re-  
 452 sulting in reduced (increased) NADW formation (Delworth and Zeng (2016)). Here we  
 453 argue that such a mechanism is present in our model simulations, resulting in an addi-  
 454 tional substantial modulation of the NH midlatitude jet location by ozone, this time via  
 455 its influence on the AMOC.

456 In particular, Figure 9 shows maps of the surface zonal wind, surface friction speed,  
 457 mixed layer depth, net heat fluxes, sea surface temperatures, and north-south heat and  
 458 salinity ocean transports over years 1-5. In response to an abrupt quadrupling of CO<sub>2</sub>,  
 459 there is a weak acceleration of the surface zonal winds on the poleward flank of the North  
 460 Atlantic jet (~60°N-70°N) (Fig. 9a, top). Over the subpolar North Atlantic the surface  
 461 winds weaken, leading to a significant reduction in surface friction speed (Fig. 9b, top)  
 462 and mixed layer depths (Fig. 9c, top), as well as increased heat flux into the ocean (in  
 463 the form of reduced latent heat fluxes out of the ocean) (Fig. 9d, top) and warmer sea  
 464 surface temperatures (Fig. 9e, top). The behavior of the heat fluxes in the subpolar gyre



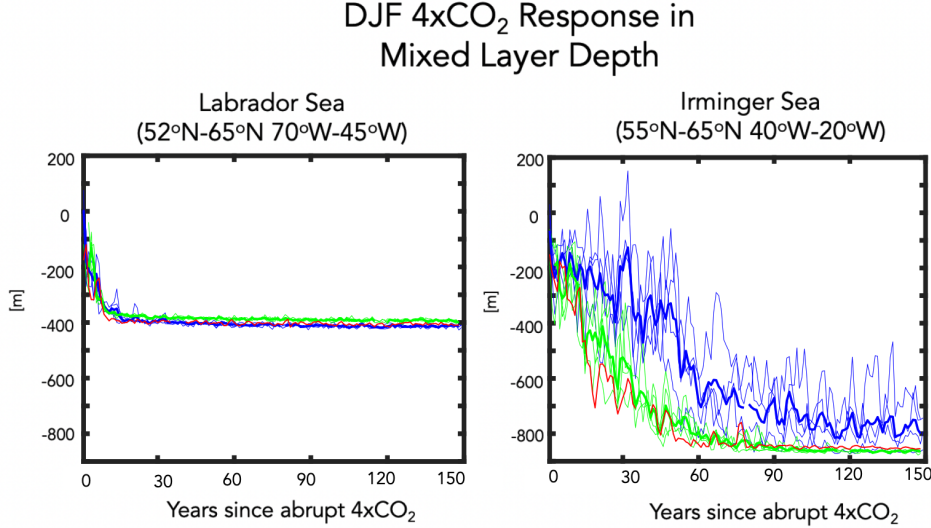


**Figure 8.** Changes in the DJF mixed layer depths, evaluated over the Labrador Sea (left) and Irminger Sea (right) in response to 4xCO<sub>2</sub>, relative to the preindustrial control simulations. Results for the LINOZ and NINT ensembles are shown in green and blue, respectively (thick lines denote ensemble means). Red lines show the response in the OMA simulation.

465 region is consistent with previous studies showing that a positive (negative) phase of the  
 466 NAO implies reduced (enhanced) atmosphere to ocean heat fluxes (Delworth et al., 2017).  
 467 At these early years the changes in meridional heat and salinity transports over the Irminger  
 468 Sea are relatively small (Fig. 9fg, top).

469 In response to the ozone changes captured in the LINOZ ensemble during years 1-  
 470 5, there is a strong reduction in the surface zonal winds and friction speed (Fig. 9 ab,  
 471 bottom), consistent with the negative NAO response evident in the 850 hPa zonal winds  
 472 (Fig. 6c, top). The surface friction changes align closely with the reduced mixed layer  
 473 depths which extend well into the Irminger Sea region and over latitudes further south  
 474 of the subpolar gyre (Fig. 9c, bottom).

475 The reductions in mixed layer depth that occur over the Irminger Sea are likely driven  
 476 by the reductions in surface wind speed which increased (primarily latent) heat fluxes  
 477 into the ocean (Fig. 9d, bottom), driving warmer sea surface temperatures in LINOZ,  
 478 relative to NINT (Fig. 9e, bottom). This pattern in heat fluxes is very similar to the NAO  
 479 heat flux composites that were prescribed in Delworth and Zeng (2016) and inferred from  
 480 observations in Ma et al. (2020), who showed that there is much greater heat loss from  
 481 the ocean over the subpolar region in association with a jet strengthening (see their Fig-  
 482 ure 6).

483 At the same time, the changes in freshwater forcing (P-E) during this time period  
 484 are negligible such that the net buoyancy forcing ( $\sim Q+F$ ) is positive. This stabilizing  
 485 buoyancy forcing from surface warming makes the mixed layer depths shallower by sup-  
 486 pressing convective mixing, shutting down NADW production (Alexander et al. (2000);  
 487 Kantha and Clayson (2000)). There is also an initial change in the north-south heat and  
 488 salt transports that is collocated with the dipole anomaly in the surface friction speed,  
 489 promoting anomalous poleward salt and heat transport into the subpolar gyre (Fig. 8fg,  
 490 bottom). This feature is confined to the top few ocean layers (not shown) and the im-

491 plied anomalous heat transport could be contributing to the warmer sea surface temper-  
 492 atures in that region, in addition to the surface heat flux changes.

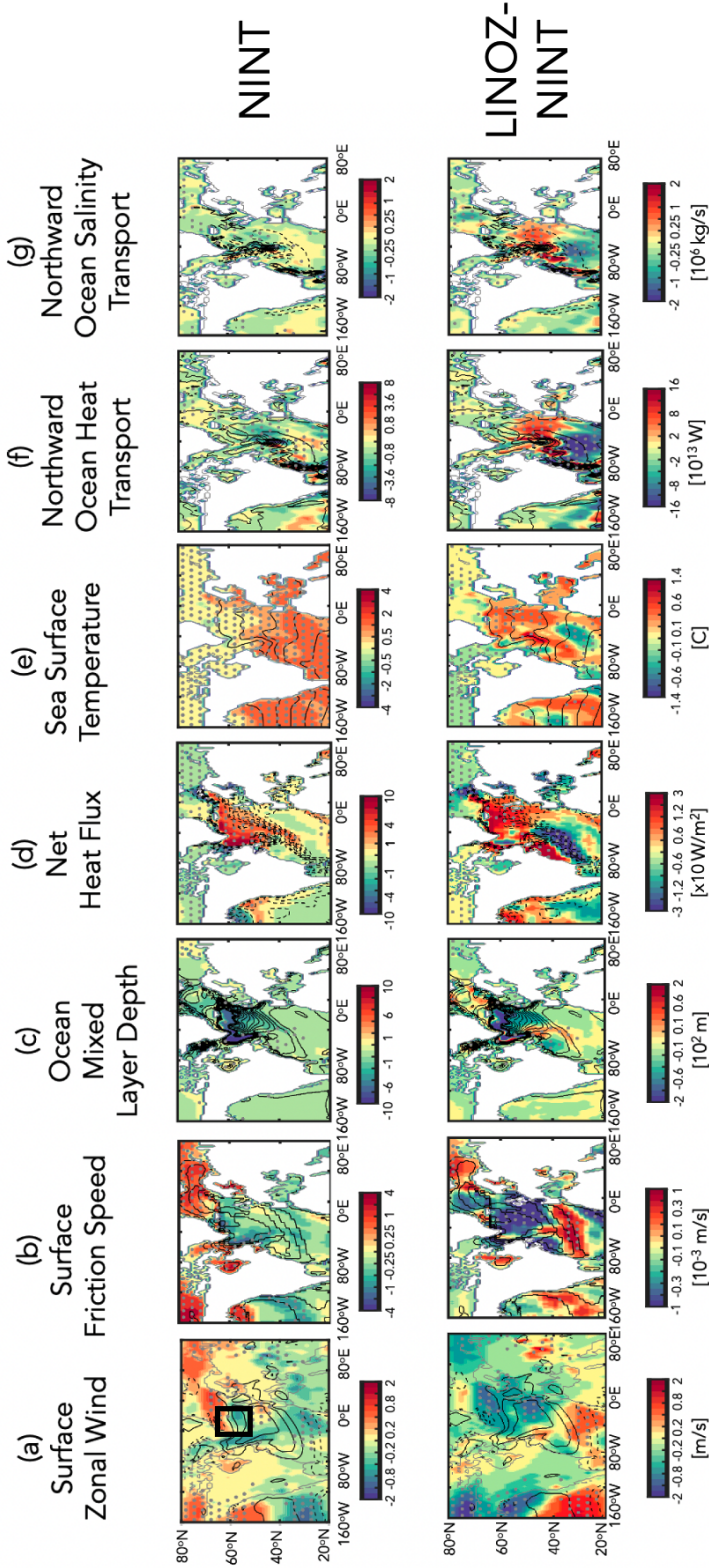
493 Over the ensuing years (5-20) a similar pattern is maintained (Figure 10, bottom).  
 494 The reduction in NADW, however, results in reduced northward heat and salinity trans-  
 495 ports (Fig. 10 fg, middle) throughout the ocean column. While this results in cooler SSTs  
 496 south of the subpolar gyre region (Fig. 10e, middle), which otherwise might enhance the  
 497 density of the near-surface water masses, the reduced northward salinity transports pre-  
 498 vent the AMOC from restarting. Interestingly, the results from the OMA simulation show  
 499 a very similar response as the LINOZ ensemble (Figure 10, bottom row), suggesting that  
 500 stratospheric ozone changes in that simulation are also the primary driver of the weaker  
 501 AMOC in that model configuration. This sequence of processes linking the surface wind  
 502 changes to anomalous heat fluxes and reduced NADW is basically identical to what is  
 503 outlined in Figure 4 of (Delworth & Zeng, 2016) and Figure 1 of (Khatri et al., 2022).  
 504 Additional analysis of the 2xCO<sub>2</sub> simulations, which feature a stronger AMOC decline  
 505 in OMA (and LINOZ) compared to NINT (Figure 2), reveals that a similar mechanism  
 506 for reduced NADW production occurs at lower CO<sub>2</sub> forcing (not shown).

507 Finally, examining the timescale of the responses of the variables shown in Figures  
 508 9 and 10 reinforces the strong coupling between the changes in surface friction speed,  
 509 sea surface temperature, latent heat fluxes and mixed layer depth changes over the Irminger  
 510 Sea region (Figure 11a-d). Despite large internal variability, there is a clear separation  
 511 between the LINOZ (OMA) and NINT simulations that emerges around year 15 (black  
 512 dashed lines). The changes in sensible heat emerge after the latent heat fluxes (Fig. 11e),  
 513 suggesting that the latter play a more important contribution in initializing the heat flux  
 514 differences in LINOZ (OMA), relative to NINT. Furthermore, while they may contribute  
 515 to enhanced positive buoyancy forcing later in the integrations, the freshwater forcing  
 516 anomalies ( $F = P - E$ ) are shown to be negligible during the initial years following the abrupt  
 517 quadrupling of CO<sub>2</sub> (Fig. 11f), indicating that the primary driver of the initial differ-  
 518 ence between the LINOZ (OMA) and NINT runs is related to the surface wind-driven  
 519 changes as they impact the latent heat fluxes into the ocean. This is consistent with Roach  
 520 et al. (2022) who showed a much stronger correlation between AMOC strength at 26°N  
 521 and the heat component of the surface buoyancy flux, relative to the freshwater com-  
 522 ponent, in various experiments using the Community Earth System Model version 1 (CESM1)  
 523 in which the winds over the subpolar gyre were nudged to reanalysis values. Note that  
 524 in our model other potential contributors to freshwater forcing from sea ice do reveal dif-  
 525 ferences between the LINOZ, OMA and NINT ensembles, but these emerge several years  
 526 (i.e., years ~20-30) after the changes in sea surface temperatures and heat fluxes (not  
 527 shown).

### 528 3.7 Ozone Driver of AMOC Changes: Fixed SST Results

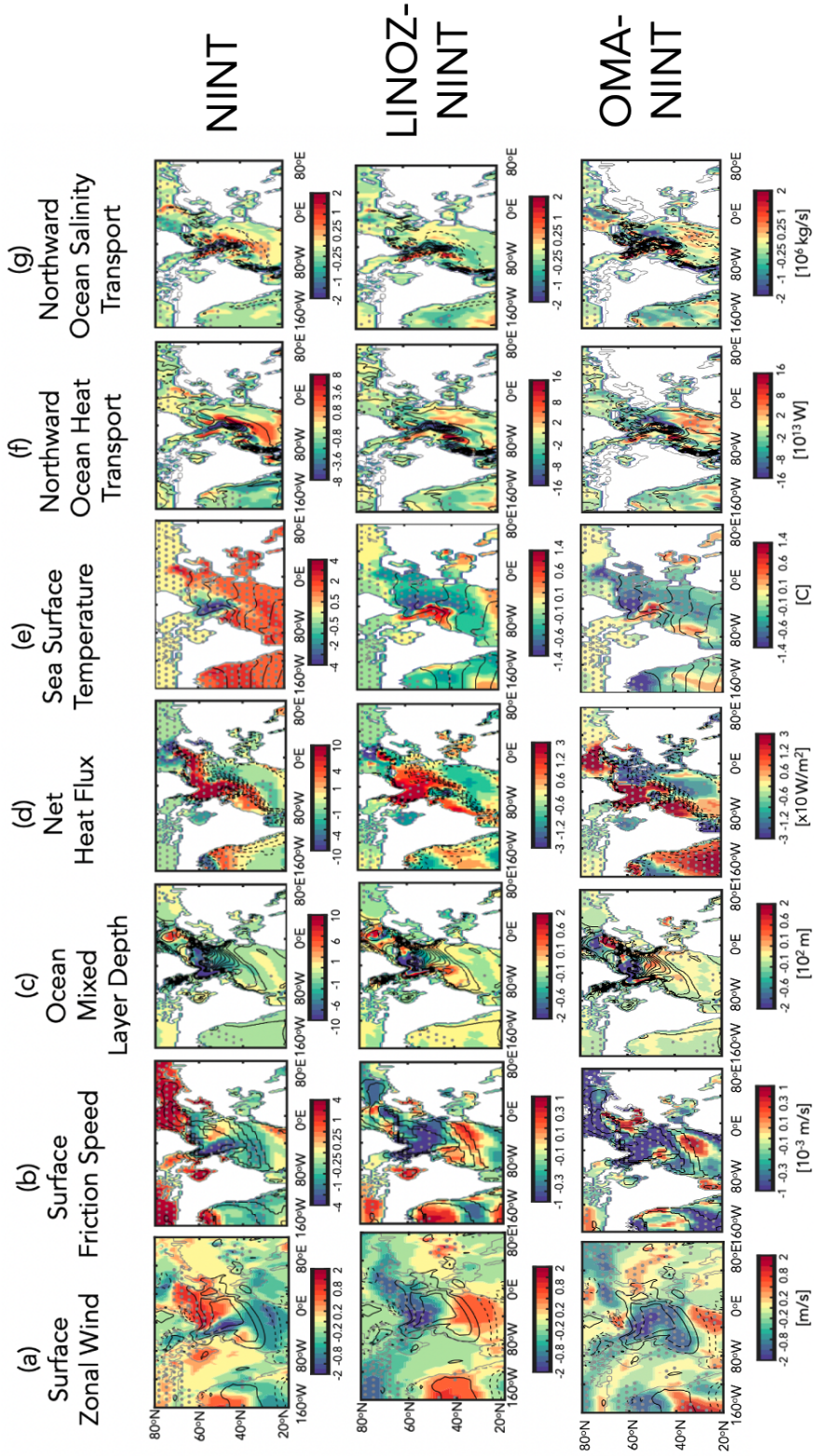
529 So far, we have shown that the stratospheric ozone changes that occur in response  
 530 to 4xCO<sub>2</sub> result in a negative NAO response over the North Atlantic (Fig. 5,6). In our  
 531 model this triggers a more rapid decline of the AMOC (Fig. 7) through surface-wind driven  
 532 changes in heat fluxes into the ocean (Fig. 9,10). While the time series analysis (Fig. 11)  
 533 reveals that the AMOC changes in the LINOZ (OMA) ensemble occur on similar timescales  
 534 as the wind (and heat flux) changes, one potentially confounding factor is the fact that  
 535 the AMOC reduction itself results in reduced wind speeds over the subpolar gyre region.  
 536 These reduced near-surface winds are associated with an anomalous anticyclonic flow  
 537 pattern (Appendix Figure 3, top) (Gervais et al. (2019); Romanou et al. (Under Review);  
 538 Orbe et al. (Under Review)), which could contribute to the reduced heat fluxes and sub-  
 539 sequent changes in NADW production. Therefore, to more convincingly link the surface  
 540 wind speed changes to the stratospheric ozone changes aloft, we next examine results  
 541 from the fixed SST experiment.

# DJF 4xCO<sub>2</sub> Response over Years 1-5

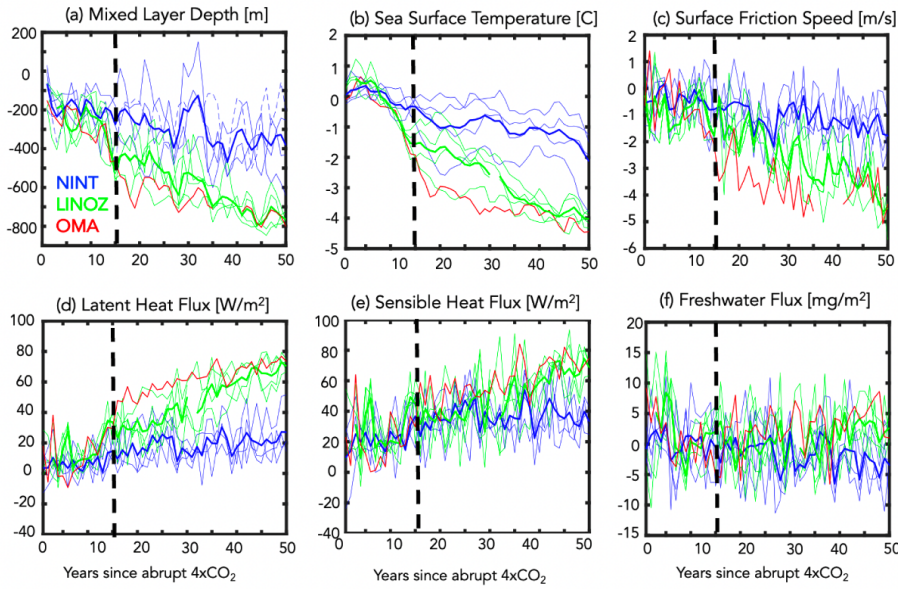


**Figure 9.** Top panels: Colors show the December-January-February (DJF) response of the surface zonal wind (a), surface friction speed (b), ocean mixed layer depth (c), net heat flux (sum of sensible plus latent heat) (d), sea surface temperature (e) and northward heat (f) and salt (g) transports in response to an abrupt quadrupling of CO<sub>2</sub>. Results are shown for the 4-member ensemble averaged NINT configuration. Bottom panels: Same as top panels, except showing the LINOZ minus NINT ensemble mean difference. For both top and bottom panels, responses have been averaged over years 1-5 since “branching” from the preindustrial control simulation. Stippled regions are statistically significant and black contours denote climatological mean DJF values. Contour intervals: surface zonal wind [2 m/s], surface friction speed [ $2.5 \times 10^{-3}$  m/s], mixed layer depth [60 m], net heat flux [ $30 \text{ W/m}^2$ ], sea surface temperature interval [2 C], northward heat flux [ $2 \times 10^{12}$  W], and northward salt flux [ $10^6$  kg/s]. The black box in (a) bounds the Irminger Sea region over which the spatial averages in Figure 8b and Figure 11 are evaluated.

# DJF 4xCO<sub>2</sub> Response over Years 5-20



**Figure 10.** Same as Figure 9, except showing the responses, averaged over years 5-20. An extra row at the bottom has been added, showing the OMA - NINT differences, where the ensemble members shown in Figures 1, 2 and 3 have been used. Same contour intervals and colorbars have been used as in Fig. 9.

DJF 4xCO<sub>2</sub> Response over Irminger Sea

**Figure 11.** Changes in the DJF mixed layer depths (a), sea surface temperatures (b), surface friction speed (c), latent heat fluxes (d), sensible heat fluxes (e) and precipitation minus evaporation (f) in response to 4xCO<sub>2</sub>, relative to the preindustrial control simulations. Averages are over the Irminger Sea (55°N-65°N, 40°W-20°W). Results for the LINOZ and NINT ensembles are shown in green and blue, respectively (thick lines denote ensemble means). Red lines show the response in the OMA simulation. Black vertical lines indicate year ~15 at which point the mixed layer depth responses in the LINOZ and NINT ensembles diverge. Note that the freshwater flux unit of 1 mg/m<sup>2</sup> per second ( $\equiv$  0.0864 mm/day  $\equiv$  3.1 cm/year) is used, because at 5°C it contributes approximately the same ocean density flux as the heat flux unit of 1 W/m<sup>2</sup> (Large and Yeager (2009)).

Figure 12 shows the ozone-induced zonal wind and temperature changes averaged over the last twenty years of the fixed SST and SIC experiments in which the ensemble mean ozone  $4xCO_2$  evolution from LINOZ is prescribed (Fig. 12 a,b). Recall that in the fixed SST experiment, only the ozone evolution differs from the preindustrial control simulation, as  $CO_2$ , SSTs and SIC are all set to preindustrial values. Comparisons with results from the fully coupled LINOZ “fast” response (see Fig. 5a,c) reveal a very similar picture. This similarity between the fully coupled fast response and the fixed SST and SIC experiment is striking, both featuring a similar change in the NH jet associated with enhanced temperature gradients in the lower stratosphere as first reported in CP2019.

Comparisons of the 850 hPa zonal winds and surface temperatures over the North Atlantic (Fig. 12c,d) also reveal a strikingly similar response between the fully coupled ensemble and the fixed SST experiment (compare with Fig. 6a,c). Note this similar response extends to sea level pressure as well (Appendix Figure 3). This result is interesting as it suggests that over the North Atlantic stratospheric ozone changes alone can result in a significant reduction in the near surface winds that is on the same order (if not larger than) the  $4xCO_2$  response. In our model this additionally results in heat flux changes that are large enough to reduce NADW production, resulting in a significant (i.e. 30-40%) change in AMOC strength.

## 4 Conclusions

Here we have used the NASA GISS coupled atmosphere-ocean high-top model (E2-2-G) to examine how coupled changes in stratospheric ozone and the ocean circulation both influence the  $4xCO_2$  response of the NH midlatitude jet. Our key results are as follows:

1. The NH midlatitude jet response to  $4xCO_2$  is modulated by coupled feedbacks from both stratospheric ozone and the AMOC, which occur of “fast” (5-20 year) and “long” (100-150 year) timescales, respectively.

2. In the “fast” response, the zonal mean jet weakens (strengthens) on its poleward (equatorward) flank, consistent with reduced LS temperature gradients associated with ozone loss. Zonally, this jet change is expressed as a negative NAO-like pattern, consisting of weaker zonal surface winds over the North Atlantic, consistent with the findings in CP2019.

3. The weaker winds over the North Atlantic are associated with increased (primarily latent) heat fluxes into the ocean which initially result in warmer SSTs over the subpolar gyre region, reducing NADW production leading to more rapid weakening of the AMOC.

4. A reduced AMOC leads to widespread cooling over the Arctic which enhance mid-to-lower tropospheric temperature gradients, resulting in a poleward shift of the NH midlatitude jet. This “long” response is consistent with previous studies showing that a weakening of the AMOC results in a stronger and poleward shifted jet in the NH (e.g., Bellomo et al. (2021); Orbe et al. (Under Review); Liu et al. (2020); Zhang et al. (Submitted)).

Taken together, conclusions 1-4 indicate that the stratospheric ozone feedback on the NH midlatitude jet reported in CP2019 depends sensitively on the behavior of the AMOC during the “fast” response, wherein the jet weakens over the North Atlantic. In our model, this wind response extends to the surface, resulting in reduced heat fluxes out of the subpolar gyre region and a more rapid decline in the AMOC. On longer timescales, these changes in the AMOC subsequently drive a poleward shift in the NH midlatitude jet. While CP2019 identified a jet change mirroring that of the “fast” response documented here, the “long” response timescale response has not been previously reported, to the

## LINOZ – NINT Fixed SST Changes

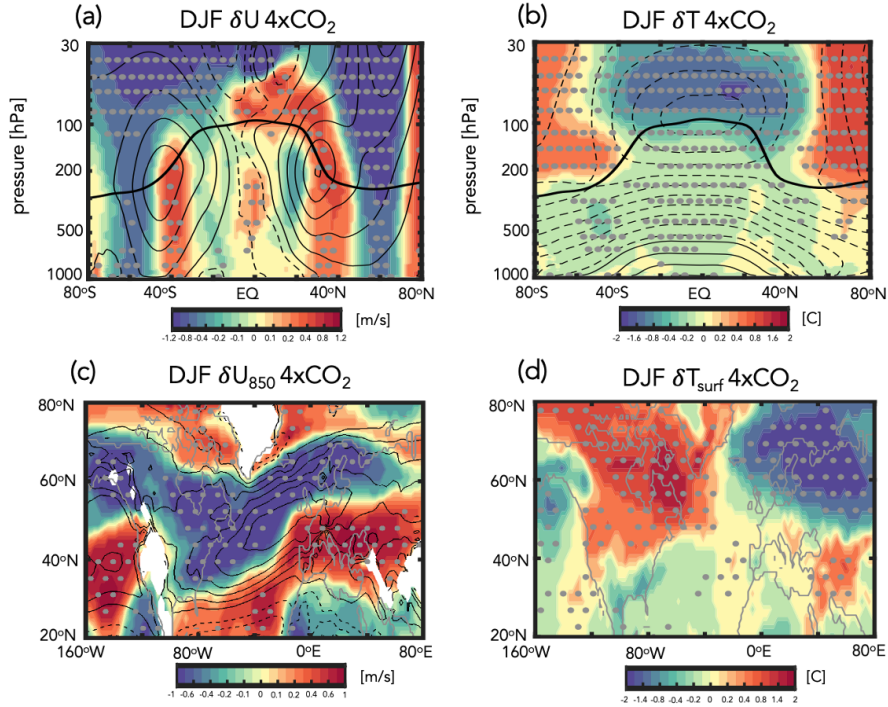


**Figure 12.** Top panels: Colors show the 4xCO<sub>2</sub> ensemble mean response in zonal mean zonal winds,  $U$  (a), temperatures,  $T$  (b), 850 hPa zonal winds,  $U_{850}$  (c) and surface temperature,  $T_{surf}$  (d) in the AMIP experiments in which the time-evolving 4xCO<sub>2</sub> ensemble mean LINOZ ozone response is prescribed. Note that SSTs, SICs and background CO<sub>2</sub> are all set to preindustrial values. Averages are shown over the last 20 years (years 40-60) of the integrations. Black contours, where shown, denote climatological mean DJF values ( $U$  contour interval: 8 m/s;  $T$  contour interval: 10 C;  $U_{850}$  contour interval: 2 m/s). Stippled regions are statistically significant and the black thick line in the top panels shows the climatological mean tropopause in the preindustrial control simulation.

591 best of our knowledge. This may reflect the fact that many of the stratosphere resolv-  
592 ing chemistry climate models that are used to inform future projections of stratospheric  
593 ozone (Eyring et al. (2008); Fahey et al. (2018)), are not always run coupled to an in-  
594 teractive ocean (Morgenstern et al. (2017)). Among those that are run coupled to a dy-  
595 namic ocean, our results will, of course, need to be tested to assess robustness.

596 Another intriguing result from this study is that the stronger decline of the AMOC  
597 occurring in the LINOZ ensemble does not appear to be a random occurrence. Rather,  
598 in our model, the “fast” ozone and “long” AMOC feedbacks on the NH jet are coupled  
599 through surface-wind driven changes in heat fluxes into the ocean. Key here is the fact  
600 that this sensitivity in the AMOC is driven only by changes in stratospheric ozone, which  
601 we have isolated from changes in other trace gases and aerosols. Thus, while previous  
602 studies (Rind et al. (2018)) have identified an important influence of interactive com-  
603 position on the AMOC, they have mainly implicated the indirect effect of aerosols on  
604 clouds through changes in sea surface temperatures and how these impact P-E (and net  
605 surface freshwater forcing). To the best of our knowledge, no study has previously demon-  
606 strated an impact of stratospheric ozone changes alone on the AMOC response to a qua-  
607 drupling of CO<sub>2</sub>. Despite the different mechanisms at play, however, are results are con-  
608 sistent with those from Rind et al. (2018) in highlighting the need for renewed focus on  
609 surface flux observations to help assess overturning stability.

610 An important caveat with our results is related to known biases in vertical mix-  
611 ing and NADW production in the ocean component of the GISS model (Miller et al. (2021);  
612 Romanou et al. (Under Review)) which likely explain why the low-top version of the cou-  
613 pled atmosphere-ocean climate model (E2-1-G) exhibits a more sensitive AMOC response  
614 to a quadrupling of CO<sub>2</sub>, compared to some other models (Bellomo et al. (2021)). At  
615 the same time, the high-top model employed in this study is much less sensitive, as the  
616 AMOC weakens by ~10 SV in response to 4xCO<sub>2</sub>, compared to a complete collapse in  
617 E2-1-G (see Figure 31 in Rind et al. (2020)). That study showed that this may be re-  
618 lated to differences in the parameterization of rainfall evaporation associated with moist  
619 convective precipitation, which they show has a strong influence on the AMOC sensi-  
620 tivity in ModelE via its effect on moisture loading in the atmosphere. While an exhaus-  
621 tive comparison between the models is beyond the scope of this study, the relevant point  
622 here is that the 4xCO<sub>2</sub> AMOC response simulated in the E2-2-G NINT ensemble is well  
623 within the CMIP5 and CMIP6 ranges documented in Mitevski et al. (2021) (see their  
624 Supplementary Figure S3).

625 Finally, our results linking the fast timescale jet response to the ensuing AMOC  
626 changes underscore the profound impact that changes in lower stratospheric winds alone  
627 can have on surface climate, as highlighted in Sigmond and Scinocca (2010). Quite re-  
628 markably, our fixed SST and SIC experiment showed that these lower stratospheric wind  
629 changes are driven primarily by changes in ozone and not by background changes in CO<sub>2</sub>  
630 or in sea surface boundary conditions. Taken together, our results suggest that more at-  
631 tention needs to be paid to understanding the time-evolving response of the coupled Earth  
632 system to future ozone changes, with a focus on changes in ocean heat transport and how  
633 these feed back on the NH jet stream.

## 634 **Appendix A Appendix Figures**

### 635 **Open Research Section**

636 This section MUST contain a statement that describes where the data supporting  
637 the conclusions can be obtained. Data cannot be listed as “Available from authors” or  
638 stored solely in supporting information. Citations to archived data should be included  
639 in your reference list. Wiley will publish it as a separate section on the paper’s page. Ex-



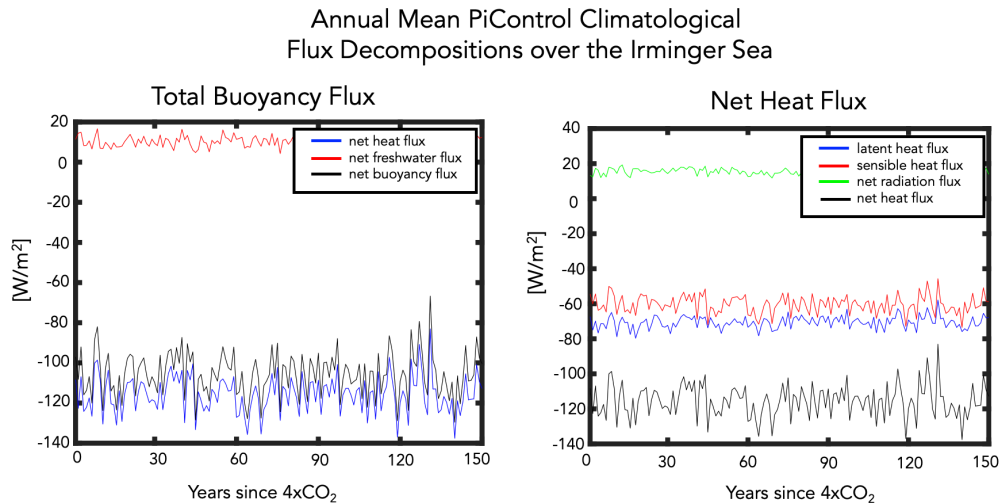


**Figure A1.** Left: Decomposition of the net surface buoyancy flux (black) into its contributions from net heat (blue) and net freshwater (red) fluxes. Right: Further decomposition of the net surface heat flux (black) into contributions from latent heat fluxes ( $Q_E$  (blue)), sensible heat fluxes ( $Q_H$  (red)), and combined solar and longwave radiative fluxes ( $Q_S+Q_L$  (green)). Results are shown for 150 years of the NINT preindustrial control simulation, evaluated over the Irminger Sea.

640 samples and complete information are here: <https://www.agu.org/Publish with AGU/Publish/Author>  
641 Resources/Data for Authors

## 642 Acknowledgments

643 Enter acknowledgments here. This section is to acknowledge funding, thank colleagues,  
644 enter any secondary affiliations, and so on.

## 645 References

- 646 Alexander, M. A., Scott, J. D., & Deser, C. (2000). Processes that influence sea sur-  
647 face temperature and ocean mixed layer depth variability in a coupled model.  
648 *Journal of Geophysical Research: Oceans*, *105*(C7), 16823–16842.
- 649 Ayarzagüena, B., Charlton-Perez, A. J., Butler, A. H., Hitchcock, P., Simpson, I. R.,  
650 Polvani, L. M., . . . others (2020). Uncertainty in the response of sudden  
651 stratospheric warmings and stratosphere-troposphere coupling to quadrupled  
652 co2 concentrations in cmip6 models. *Journal of Geophysical Research: Atmo-*  
653 *spheres*, *125*(6), e2019JD032345.
- 654 Bauer, S. E., Tsigaridis, K., Faluvegi, G., Kelley, M., Lo, K. K., Miller, R. L., . . .  
655 Wu, J. (2020). Historical (1850–2014) aerosol evolution and role on climate  
656 forcing using the giss modele2. 1 contribution to cmip6. *Journal of Advances*  
657 *in Modeling Earth Systems*, *12*(8), e2019MS001978.
- 658 Bellomo, K., Angeloni, M., Corti, S., & von Hardenberg, J. (2021). Future climate  
659 change shaped by inter-model differences in atlantic meridional overturning  
660 circulation response. *Nature Communications*, *12*(1), 1–10.
- 661 Booth, B. B., Dunstone, N. J., Halloran, P. R., Andrews, T., & Bellouin, N. (2012).  
662 Aerosols implicated as a prime driver of twentieth-century north atlantic cli-  
663 mate variability. *Nature*, *484*(7393), 228–232.

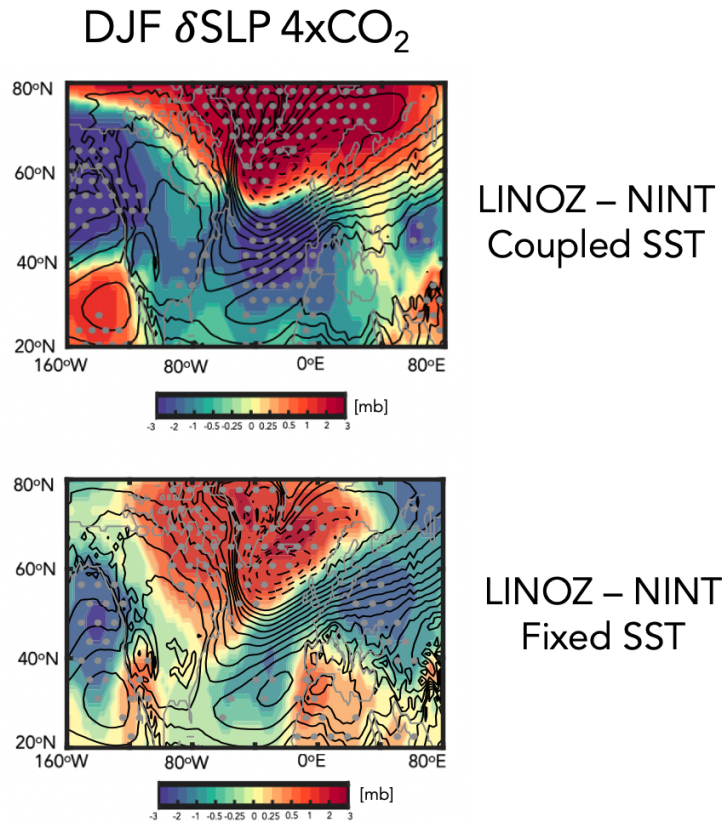


**Figure A2.** Top panel: Colors show the LINOZ minus NINT ensemble mean difference in the December-January-February (DJF) “fast” response of the sea level pressure in response to an abrupt quadrupling of  $\text{CO}_2$ . Results are shown for the fully coupled atmosphere-ocean simulations. Bottom panel: The response in sea level pressure in the AMIP experiments in which the time-evolving  $4\times\text{CO}_2$  ensemble mean LINOZ ozone response is prescribed. Note that SSTs, SICs and background  $\text{CO}_2$  are set to preindustrial values. Black contours denote climatological mean DJF values (contour interval: 10 mb). Stippled regions are statistically significant.

- 664 Butler, A. H., Thompson, D. W., & Heikes, R. (2010). The steady-state atmospheric  
665 circulation response to climate change-like thermal forcings in a simple general  
666 circulation model. *Journal of Climate*, *23*(13), 3474–3496.
- 667 Ceppi, P., & Hartmann, D. L. (2015). Connections between clouds, radiation, and  
668 midlatitude dynamics: A review. *Current Climate Change Reports*, *1*(2), 94–  
669 102.
- 670 Ceppi, P., Zappa, G., Shepherd, T. G., & Gregory, J. M. (2018). Fast and slow com-  
671 ponents of the extratropical atmospheric circulation response to co2 forcing.  
672 *Journal of Climate*, *31*(3), 1091–1105.
- 673 Chiodo, G., Polvani, L. M., Marsh, D. R., Stenke, A., Ball, W., Rozanov, E., ...  
674 Tsigaridis, K. (2018). The response of the ozone layer to quadrupled co2  
675 concentrations. *Journal of Climate*, *31*(10), 3893–3907.
- 676 Cowan, T., & Cai, W. (2013). The response of the large-scale ocean circulation  
677 to 20th century asian and non-asian aerosols. *Geophysical Research Letters*,  
678 *40*(11), 2761–2767.
- 679 DallaSanta, K., Orbe, C., Rind, D., Nazarenko, L., & Jonas, J. (2021a). Dynamical  
680 and trace gas responses of the quasi-biennial oscillation to increased co2. *Jour-  
681 nal of Geophysical Research: Atmospheres*, *126*(6), e2020JD034151.
- 682 DallaSanta, K., Orbe, C., Rind, D., Nazarenko, L., & Jonas, J. (2021b). Response of  
683 the quasi-biennial oscillation to historical volcanic eruptions. *Geophysical Re-  
684 search Letters*, *48*(20), e2021GL095412.
- 685 Delworth, T. L., & Dixon, K. W. (2000). Implications of the recent trend in the  
686 arctic/north atlantic oscillation for the north atlantic thermohaline circulation.  
687 *Journal of Climate*, *13*(21), 3721–3727.
- 688 Delworth, T. L., & Zeng, F. (2016). The impact of the north atlantic oscillation on  
689 climate through its influence on the atlantic meridional overturning circulation.  
690 *Journal of Climate*, *29*(3), 941–962.
- 691 Delworth, T. L., Zeng, F., Zhang, L., Zhang, R., Vecchi, G. A., & Yang, X. (2017).  
692 The central role of ocean dynamics in connecting the north atlantic oscillation  
693 to the extratropical component of the atlantic multidecadal oscillation. *Journal  
694 of Climate*, *30*(10), 3789–3805.
- 695 Eyring, V., Bony, S., Meehl, G. A., Senior, C. A., Stevens, B., Stouffer, R. J., &  
696 Taylor, K. E. (2016). Overview of the coupled model intercomparison project  
697 phase 6 (cmip6) experimental design and organization. *Geoscientific Model  
698 Development*, *9*(5), 1937–1958.
- 699 Eyring, V., Chipperfield, M., Giorgetta, M. A., Kinnison, D. E., Manzini, E.,  
700 Matthes, K., ... Waugh, D. W. (2008). Overview of the new ccmval refer-  
701 ence and sensitivity simulations in support of upcoming ozone and climate  
702 assessments and the planned sparcc ccmval report. *SPARC newsletter*, *30*,  
703 20–26.
- 704 Fahey, D., Newman, P. A., Pyle, J. A., Safari, B., Chipperfield, M. P., Karoly, D.,  
705 ... Doherty, S. J. (2018). *Scientific assessment of ozone depletion: 2018, global  
706 ozone research and monitoring project-report no. 58*. World Meteorological Or-  
707 ganization.
- 708 Garcia, R. R., & Randel, W. J. (2008). Acceleration of the brewer–dobson circula-  
709 tion due to increases in greenhouse gases. *Journal of the Atmospheric Sciences*,  
710 *65*(8), 2731–2739.
- 711 Gervais, M., Shaman, J., & Kushnir, Y. (2019). Impacts of the north atlantic warm-  
712 ing hole in future climate projections: Mean atmospheric circulation and the  
713 north atlantic jet. *Journal of Climate*, *32*(10), 2673–2689.
- 714 Grise, K. M., & Polvani, L. M. (2014). The response of midlatitude jets to increased  
715 co2: Distinguishing the roles of sea surface temperature and direct radiative  
716 forcing. *Geophysical Research Letters*, *41*(19), 6863–6871.
- 717 Isaksen, I. S., Granier, C., Myhre, G., Berntsen, T., Dalsøren, S. B., Gauss, M., ...  
718 others (2009). Atmospheric composition change: Climate–chemistry interac-

- 719 tions. *Atmospheric Environment*, *43*(33), 5138–5192.
- 720 Kantha, L. H., & Clayson, C. A. (2000). *Small scale processes in geophysical fluid*  
721 *flows*. Elsevier.
- 722 Khatri, H., Williams, R. G., Woollings, T., & Smith, D. M. (2022). Fast and slow  
723 subpolar ocean responses to the north atlantic oscillation: Thermal and dy-  
724 namical changes. *Geophysical Research Letters*, *49*(24), e2022GL101480.
- 725 Lindzen, R. S. (1987). On the development of the theory of the qbo. *Bulletin of the*  
726 *American Meteorological Society*, 329–337.
- 727 Liu, W., Fedorov, A. V., Xie, S.-P., & Hu, S. (2020). Climate impacts of a weak-  
728 ened atlantic meridional overturning circulation in a warming climate. *Science*  
729 *advances*, *6*(26), eaaz4876.
- 730 Ma, L., Woollings, T., Williams, R. G., Smith, D., & Dunstone, N. (2020). How  
731 does the winter jet stream affect surface temperature, heat flux, and sea ice in  
732 the north atlantic? *Journal of Climate*, *33*(9), 3711–3730.
- 733 Marshall, J., Johnson, H., & Goodman, J. (2001). A study of the interaction of  
734 the north atlantic oscillation with ocean circulation. *Journal of Climate*, *14*(7),  
735 1399–1421.
- 736 McLinden, C., Olsen, S., Hannegan, B., Wild, O., Prather, M., & Sundet, J.  
737 (2000). Stratospheric ozone in 3-d models: A simple chemistry and the cross-  
738 tropopause flux. *Journal of Geophysical Research: Atmospheres*, *105*(D11),  
739 14653–14665.
- 740 Miller, R. L., Schmidt, G. A., Nazarenko, L. S., Bauer, S. E., Kelley, M., Ruedy, R.,  
741 ... others (2021). Cmp6 historical simulations (1850–2014) with giss-e2. 1.  
742 *Journal of Advances in Modeling Earth Systems*, *13*(1), e2019MS002034.
- 743 Mitevski, I., Orbe, C., Chemke, R., Nazarenko, L., & Polvani, L. M. (2021). Non-  
744 monotonic response of the climate system to abrupt co2 forcing. *Geophysical*  
745 *research letters*, *48*(6), e2020GL090861.
- 746 Morgenstern, O., Hegglin, M. I., Rozanov, E., O’Connor, F. M., Abraham, N. L.,  
747 Akiyoshi, H., ... others (2017). Review of the global models used within  
748 phase 1 of the chemistry–climate model initiative (ccmi). *Geoscientific Model*  
749 *Development*, *10*(2), 639–671.
- 750 Nowack, P. J., Luke Abraham, N., Maycock, A. C., Braesicke, P., Gregory, J. M.,  
751 Joshi, M. M., ... Pyle, J. A. (2015). A large ozone-circulation feedback and  
752 its implications for global warming assessments. *Nature climate change*, *5*(1),  
753 41–45.
- 754 O’Callaghan, M. J. D. S., Ameen, & Mitchell, D. (2014). The effects of different sud-  
755 den stratospheric warming types on the ocean. *Geophysical Research Letters*,  
756 *41*(21), 7739–7745.
- 757 Orbe, C., Rind, D., Jonas, J., Nazarenko, L., Faluvegi, G., Murray, L. T., ... oth-  
758 ers (2020). Giss model e2. 2: A climate model optimized for the middle  
759 atmosphere—2. validation of large-scale transport and evaluation of cli-  
760 mate response. *Journal of Geophysical Research: Atmospheres*, *125*(24),  
761 e2020JD033151.
- 762 Orbe, C., Rind, D., Miller, R., Nazarenko, L., Romanou, A., Jonas, J., ... Schmidt,  
763 G. (Under Review). Atmospheric response to a collapse of the north atlantic  
764 circulation under a mid-range future climate scenario: A regime shift in north-  
765 ern hemisphere dynamics. *Journal of Climate*.
- 766 Reichler, T., Kim, J., Manzini, E., & Kröger, J. (2012). A stratospheric connection  
767 to atlantic climate variability. *Nature Geoscience*, *5*(11), 783–787.
- 768 Rind, D., Jonas, J., Balachandran, N., Schmidt, G. A., & Lean, J. (2014). The  
769 qbo in two giss global climate models: 1. generation of the qbo. *Journal of*  
770 *Geophysical Research: Atmospheres*, *119*(14), 8798–8824.
- 771 Rind, D., Orbe, C., Jonas, J., Nazarenko, L., Zhou, T., Kelley, M., ... others  
772 (2020). Giss model e2. 2: A climate model optimized for the middle atmo-  
773 sphere—model structure, climatology, variability, and climate sensitivity.

- 774 *Journal of Geophysical Research: Atmospheres*, 125(10), e2019JD032204.
- 775 Rind, D., Schmidt, G. A., Jonas, J., Miller, R., Nazarenko, L., Kelley, M., & Roman-
- 776 ski, J. (2018). Multicentury instability of the atlantic meridional circulation in
- 777 rapid warming simulations with giss modele2. *Journal of Geophysical Research:*
- 778 *Atmospheres*, 123(12), 6331–6355.
- 779 Rind, D., Suozzo, R., Balachandran, N., Lacis, A., & Russell, G. (1988). The giss
- 780 global climate-middle atmosphere model. part i: Model structure and climatol-
- 781 ogy. *Journal of the atmospheric sciences*, 45(3), 329–370.
- 782 Roach, L. A., Blanchard-Wrigglesworth, E., Ragen, S., Cheng, W., Armour, K. C.,
- 783 & Bitz, C. M. (2022). The impact of winds on amoc in a fully-coupled climate
- 784 model. *Geophysical Research Letters*, e2022GL101203.
- 785 Romanou, A., Rind, D., Jonas, J., Miller, R., Kelley, M., Russel, G., ... Schmidt,
- 786 G. A. (Under Review). Stochastic bifurcation of the North Atlantic circula-
- 787 tion under a mid-range future climate scenario with the NASA-GISS ModelE.
- 788 *Journal of Climate*.
- 789 Shaw, T., Baldwin, M., Barnes, E. A., Caballero, R., Garfinkel, C., Hwang, Y.-T.,
- 790 ... others (2016). Storm track processes and the opposing influences of climate
- 791 change. *Nature Geoscience*, 9(9), 656–664.
- 792 Shaw, T. A. (2019). Mechanisms of future predicted changes in the zonal mean mid-
- 793 latitude circulation. *Current Climate Change Reports*, 5(4), 345–357.
- 794 Shepherd, T. G. (2014). Atmospheric circulation as a source of uncertainty in cli-
- 795 mate change projections. *Nature Geoscience*, 7(10), 703–708.
- 796 Sigmond, M., & Scinocca, J. F. (2010). The influence of the basic state on the
- 797 northern hemisphere circulation response to climate change. *Journal of Cli-*
- 798 *mate*, 23(6), 1434–1446.
- 799 Simpson, I. R., Shaw, T. A., & Seager, R. (2014). A diagnosis of the seasonally
- 800 and longitudinally varying midlatitude circulation response to global warming.
- 801 *Journal of the Atmospheric Sciences*, 71(7), 2489–2515.
- 802 Smith, D. M., Screen, J. A., Deser, C., Cohen, J., Fyfe, J. C., García-Serrano, J.,
- 803 ... others (2019). The polar amplification model intercomparison project
- 804 (pamip) contribution to cmip6: investigating the causes and consequences of
- 805 polar amplification. *Geoscientific Model Development*, 12(3), 1139–1164.
- 806 Swingedouw, D., Ortega, P., Mignot, J., Guilyardi, E., Masson-Delmotte, V., But-
- 807 tler, P. G., ... Séférian, R. (2015). Bidecadal north atlantic ocean circulation
- 808 variability controlled by timing of volcanic eruptions. *Nature communications*,
- 809 6(1), 1–12.
- 810 Vallis, G. K., Zurita-Gotor, P., Cairns, C., & Kidston, J. (2015). Response of the
- 811 large-scale structure of the atmosphere to global warming. *Quarterly Journal*
- 812 *of the Royal Meteorological Society*, 141(690), 1479–1501.
- 813 Visbeck, M., Cullen, H., Krahlmann, G., & Naik, N. (1998). An ocean model’s re-
- 814 sponse to north atlantic oscillation-like wind forcing. *Geophysical research let-*
- 815 *ters*, 25(24), 4521–4524.
- 816 Voigt, A., & Shaw, T. A. (2015). Circulation response to warming shaped by radi-
- 817 ative changes of clouds and water vapour. *Nature Geoscience*, 8(2), 102–106.
- 818 Yuval, J., & Kaspi, Y. (2020). Eddy activity response to global warming-like tem-
- 819 perature changes. *Journal of Climate*, 33(4), 1381–1404.
- 820 Zhai, H. L. J., Xiaoming, & Marshall, D. P. (2014). A simple model of the response
- 821 of the atlantic to the north atlantic oscillation. *Journal of Climate*, 27(11),
- 822 4052–4069.
- 823 Zhang, X., Waugh, D., & Orbe, C. (Submitted). Response of Tropospheric Ttrans-
- 824 port to Abrupt CO2 Increase: D]ependence on the Atlantic Meridional Over-
- 825 turning Circulation. *Journal of Geophysical Research: Atmospheres*.